

See discussions, stats, and author profiles for this publication at: <https://www.researchgate.net/publication/11140415>

Kinetic Mechanism of Direct Transfer of Escherichia coli SSB Tetramers between Single-Stranded DNA Molecules †

ARTICLE in BIOCHEMISTRY · OCTOBER 2002

Impact Factor: 3.02 · DOI: 10.1021/bi020361m · Source: PubMed

CITATIONS

41

READS

9

2 AUTHORS:



Alexander G Kozlov

Washington University in St. Louis

34 PUBLICATIONS 1,366 CITATIONS

SEE PROFILE



Timothy M. Lohman

Washington University in St. Louis

189 PUBLICATIONS 12,003 CITATIONS

SEE PROFILE

Kinetic Mechanism of Direct Transfer of *Escherichia coli* SSB Tetramers between Single-Stranded DNA Molecules[†]

Alexander G. Kozlov and Timothy M. Lohman*

Department of Biochemistry and Molecular Biophysics, Washington University School of Medicine, 660 South Euclid Avenue, St. Louis, Missouri 63110

Received May 15, 2002; Revised Manuscript Received July 10, 2002

ABSTRACT: The kinetic mechanism of transfer of the homotetrameric *Escherichia coli* SSB protein between ssDNA molecules was studied using stopped-flow experiments. Dissociation of SSB from the donor ssDNA was monitored after addition of a large excess of unlabeled acceptor ssDNA by using either SSB tryptophan fluorescence or the fluorescence of a ssDNA labeled with an extrinsic fluorophore [fluorescein (F) or Cy3]. The dominant pathway for SSB dissociation occurs by a “direct transfer” mechanism in which an intermediate composed of two DNA molecules bound to one SSB tetramer forms transiently prior to the release of the acceptor DNA. When an initial 1:1 SSB–ssDNA complex is formed with (dT)₇₀ in the fully wrapped (SSB)₆₅ mode so that all four SSB subunits are bound to (dT)₇₀, the formation of the ternary intermediate complex occurs slowly with an apparent bimolecular rate constant, $k_{2,app}$, ranging from $1.2 \times 10^3 \text{ M}^{-1} \text{ s}^{-1}$ (0.2 M NaCl) to $\sim 5.1 \times 10^3 \text{ M}^{-1} \text{ s}^{-1}$ (0.4 M NaBr), and this rate limits the overall rate of the transfer reaction (pH 8.1, 25 °C). These rate constants are $\sim 7 \times 10^5$ - and $\sim 7 \times 10^4$ -fold lower, respectively, than those measured for binding of the same ssDNA to an unligated SSB tetramer to form a singly ligated complex. However, when an initial SSB–ssDNA complex is formed with (dT)₃₅ so that only two SSB subunits interact with the DNA in an (SSB)₃₅ complex, the formation of the ternary intermediate occurs much faster with a $k_{2,app}$ ranging from $>6.3 \times 10^7 \text{ M}^{-1} \text{ s}^{-1}$ (0.2 M NaCl) to $2.6 \times 10^7 \text{ M}^{-1} \text{ s}^{-1}$ (0.4 M NaBr). For these experiments, the rate of dissociation of the donor ssDNA determines the overall rate of the transfer reaction. Hence, an SSB tetramer can be transferred from one ssDNA molecule to another without proceeding through a free protein intermediate, and the rate of transfer is determined by the availability of free DNA binding sites within the initial SSB–ssDNA donor complex. Such a mechanism may be used to recycle SSB tetramers between old and newly formed ssDNA regions during lagging strand DNA replication.

The *Escherichia coli* single-stranded binding protein (SSB)¹ plays essential roles in DNA replication, recombination, and repair (1, 2). *E. coli* SSB is a homotetrameric nonspecific single-stranded (ss) DNA binding protein (for reviews, see refs 3–6) that can bind long ssDNA in a number of different binding modes depending on solution conditions, especially the salt concentration and type, as well as protein to DNA ratios (7–10). Two of the major polynucleotide binding modes are the (SSB)₃₅ and (SSB)₆₅ modes, which differ by the number of nucleotides occluded per SSB tetramer. In the (SSB)₃₅ binding mode, the ssDNA interacts with only two of the SSB subunits on average, occluding ~ 35 nucleotides per tetramer. In this mode, SSB binds to long ssDNA with “unlimited” positive cooperativity such that it can form clusters of protein along the ssDNA (10–12);

this mode is favored at low monovalent salt concentrations ($<10 \text{ mM NaCl}$) and high protein to DNA ratios (high binding densities). In the (SSB)₆₅ binding mode, the ssDNA interacts with all four protein subunits, occluding ~ 65 nucleotides per tetramer. This binding mode is favored at high monovalent salt concentrations ($>0.2 \text{ M}$) or in the presence of divalent cations or polyamines (7, 8, 13) and displays a much lower cooperativity of the “limited” type such that long protein clusters are not observed (10, 11, 14, 15). The general properties of ssDNA binding of the *E. coli* SSB tetramer differ considerably from those of the phage T4 gene 32 protein, even though these are both classified as helix-destabilizing proteins (3). It has still not been determined whether both of these binding modes are functionally important in vivo; however, on the basis of their ssDNA binding properties, it has been proposed that the (SSB)₃₅ binding mode is likely to function predominantly during DNA replication, whereas the less cooperative, (SSB)₆₅ binding mode might be used during other DNA metabolic processes (3). In both of these binding modes, the SSB remains tetrameric, even when bound in the (SSB)₃₅ binding mode.

The equilibrium binding of the *E. coli* SSB tetramer to both ss polynucleotides and oligodeoxynucleotides has been

[†] This research was supported in part by the NIH (R01 GM30498).

* To whom correspondence should be addressed: Department of Biochemistry and Molecular Biophysics, Box 8231, Washington University School of Medicine, 660 S. Euclid Ave., St. Louis, MO 63110. E-mail: lohman@biochem.wustl.edu. Telephone: (314) 362-4393. Fax: (314) 362-7183.

¹ Abbreviations: SSB, single-stranded binding protein; ssDNA, single-stranded DNA; FRET, fluorescence resonance energy transfer; Tris, tris(hydroxymethyl)aminomethane; EDTA, ethylenediaminetetraacetic acid.

studied extensively (early studies are reviewed in refs 4 and 6). Studies with oligodeoxynucleotides have shown that the DNA binding sites on the SSB tetramer can be saturated with one molecule of (dX)₇₀, two molecules of (dX)₂₇ or (dX)₃₅, or four molecules of (dX)₁₆. At 0.2 M NaCl, one molecule of (dX)₇₀ interacts with all four subunits and wraps around the SSB tetramer (16, 17). These conclusions have been confirmed by the X-ray crystal structure of the SSB_C tetramer (where 40 amino acids have been removed from the C-terminus of each polypeptide) bound to two molecules of (dC)₃₅ (18), and a model has been proposed for how ssDNA wraps around the SSB tetramer in the (SSB)₆₅ binding mode. In this model, the path of the ssDNA follows that of the stitching on a baseball, with the two ends of a ssDNA 65–70 nucleotides in length brought close together. Equilibrium studies with shorter oligodeoxynucleotides [e.g., (dX)₃₅] indicate that there is a strong negative cooperativity associated with binding of the second molecule of (dX)₃₅, and this negative cooperativity becomes more pronounced as the salt concentration is decreased (16, 17).

Although we have a fairly detailed understanding of the equilibrium ssDNA binding properties of the *E. coli* SSB tetramer, the kinetics and mechanisms of binding and dissociation are much more poorly understood. Such kinetic mechanistic information is needed to understand how SSB–ssDNA complexes might form and be recycled during processes such as DNA replication, recombination, and repair. This kinetic information would also be useful in understanding the role of the SSB in studies of other enzymes in vitro, such as DNA polymerases and DNA helicases, since the SSB is used routinely in kinetic studies of these enzymes. Although there have been several previous kinetic studies of *E. coli* SSB binding to ssDNA, both polynucleotides (19–22) and oligodeoxynucleotides (23, 24), the majority of these studies were performed before it was recognized that SSB tetramers can bind ssDNA in several binding modes. We recently examined the kinetic mechanism of SSB binding to the oligodeoxythymidylates (dT)₇₀ and (dT)₃₅ and showed that binding of (dT)₇₀ to form a 1:1 fully wrapped complex occurs by a two-step process (24). Rapid initial binding with a bimolecular rate constant $k_{1,app}$ approaching 10^9 M⁻¹ s⁻¹ in the limit of low salt concentration is followed by a second step that is too rapid to measure by stopped-flow techniques in which ssDNA wraps around the tetramer. Although we demonstrated that dissociation of these complexes is very slow under nearly all the conditions that were examined, we were unable to obtain much information about the rates or mechanisms of dissociation of these complexes.

There have been several interesting suggestions made for mechanisms by which the *E. coli* SSB tetramer might be able to redistribute itself along ssDNA. On the basis of early nitrocellulose filter binding studies of the kinetics of SSB dissociation from long stretches of natural ssDNA, Schneider and Wetmur (20) suggested that SSB tetramers can be transferred from one ssDNA molecule to another without proceeding through a free SSB intermediate. Although good evidence for such “direct transfer” of SSB has been found, detailed mechanistic information about how this reaction occurs is lacking. In particular, does direct transfer occur preferentially via one DNA binding mode, or can it occur from any binding mode? What are the mechanisms and the

rates for this process, and is it functionally important for DNA metabolism? To address these questions, we have performed stopped-flow kinetic studies of the dissociation of fluorescently labeled oligodeoxythymidylates [(dT)₃₅ and (dT)₇₀] by examining the rates and mechanism by which competitor ssDNA can displace ssDNA that is prebound to the SSB tetramer under well-defined conditions that selectively favor one or the other of the different SSB binding modes so that the preformed complexes interact with ssDNA using only two subunits of the tetramer, or all four subunits of the tetramer.

MATERIALS AND METHODS

Reagents and Buffers. All solutions were prepared with reagent grade chemicals and glass-distilled water that was further treated with a Milli Q (Millipore, Bedford, MA) water purification system. Buffer T is 10 mM Tris [tris(hydroxymethyl)aminomethane] and 0.1 mM Na₃EDTA (ethylenediaminetetraacetic acid) (pH 8.1). Buffers were prepared by adjusting the pH at 25 °C with 5 M HCl of 10 mM Tris base solutions containing the indicated concentrations of NaCl or NaBr.

***E. coli* SSB and Nucleic Acids.** SSB was purified as described previously (25) with the added step of a double-stranded DNA cellulose column for removal of a minor exonuclease contaminant (26). The SSB concentration was determined spectrophotometrically in buffer T and 0.2 M NaCl using an extinction coefficient ϵ_{280} of 1.13×10^5 M⁻¹ (tetramer) cm⁻¹ (7). The SSB is a stable tetramer at all salt and protein concentrations used in this study (6, 15), and concentrations are reported as the tetramer. All oligodeoxynucleotides, including those labeled with fluorescein (F), Cy3, or Cy5 [(dT)₃₅, (dT)₇₀, F(dT)₃₅, F(dT)₇₀, Cy3(dT)₆₉, and doubly fluorescently labeled Cy5(dT)₆₅Cy3dT], were synthesized using an ABI model 391 automated DNA synthesizer (Applied Biosystems, Foster City, CA) with phosphoramidites from Glenn Research (Sterling, VA). In F(dT)₃₅, the fluorescein (F) was incorporated into the 21st position from the 5'-end of the oligodeoxynucleotide [5'-(dT)₂₀FdT-(dT)₁₄-3']; in F(dT)₇₀ and Cy3(dT)₆₉, the fluorescein and Cy3 were incorporated at the 5'-end of the oligodeoxynucleotides [5'-FdT(dT)₆₉ and 5'-Cy5(dT)₆₉]. For the doubly labeled (dT)₆₆, the fluorescent probes Cy5 and Cy3 were incorporated at the 5'- and 3'-ends of the oligonucleotide, respectively [5'-Cy5(dT)₆₅Cy3dT-3']. All oligodeoxynucleotides were purified to >99% homogeneity using polyacrylamide gel electrophoresis (PAGE) and electroelution as described previously (12). Concentrations of (dT)₃₅ and (dT)₇₀ were determined spectrophotometrically in buffer T (pH 8.1) and 0.1 M NaCl using an extinction coefficient ϵ_{260}^{dT} of 8.1×10^3 M⁻¹ (nucleotide) cm⁻¹ (27). Concentrations of the oligodeoxythymidylates labeled with fluorescent probes were determined using extinction coefficients (per mole of ssDNA molecule) at 260 nm calculated according to the expression $\epsilon_{260} = N\epsilon_{260}^{dT} + \epsilon_{260}^F + \epsilon_{260}^{Cy3} + \epsilon_{260}^{Cy5}$, where N is the number of nucleotides and $\epsilon_{260}^{dT} = 2.096 \times 10^4$ M⁻¹ cm⁻¹, $\epsilon_{260}^{Cy3} = 5 \times 10^3$ M⁻¹ cm⁻¹, and $\epsilon_{260}^{Cy5} = 1 \times 10^4$ M⁻¹ cm⁻¹ (Glen Research). All SSB and ssDNA samples were dialyzed extensively against buffer T at the indicated salt concentration at 4 °C for use in the stopped-flow kinetic experiments at 25 °C.

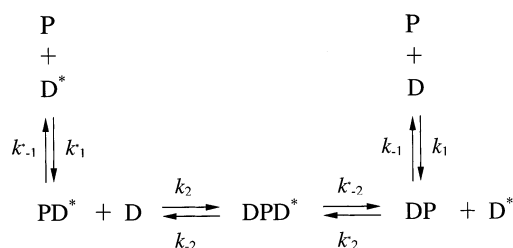
Fluorescence Titrations and Stopped-Flow Studies. Equilibrium binding of F(dT)₇₀ and Cy3(dT)₆₉ to SSB was studied by monitoring the quenching of SSB Trp fluorescence, using an SLM 8000C spectrofluorometer ($\lambda_{\text{ex}} = 296$ nm, 2 nm excitation band-pass; $\lambda_{\text{em}} = 345$ nm, 4 nm emission band-pass) as described previously (17, 24, 28). Stopped-flow experiments were performed in buffer T at 25 °C using an Applied Photophysics SX.18MV stopped-flow instrument (Applied Photophysics Ltd., Leatherhead, U.K.) supplied with a 150 W xenon arc lamp. All optical filters were from Oriel Corp. (Stratford, CT). In experiments in which the SSB Trp fluorescence was being monitored, an excitation wavelength of 296 nm was used and fluorescence emission was detected either at wavelengths of >340 nm using a long-pass filter (Oriel catalog no. 51258) or at 350 nm using an interference filter (Oriel catalog no. 53400) as indicated in the text. In experiments in which the fluorescence of ssDNA labeled with Cy3 was being monitored [Cy3(dT)₆₉], an excitation wavelength of 515 nm was used and fluorescence emission was detected using a 570 nm long-pass filter (Oriel catalog no. 51310). In experiments in which the fluorescence of ssDNA labeled with fluorescein was being monitored [F(dT)₇₀ and F(dT)₃₅], an excitation wavelength of 496 nm was used and fluorescence emission was detected using a 530 nm long-pass filter (Oriel catalog no. 51300). In the FRET (fluorescence resonance energy transfer) experiments with Cy5(pT)₆₅Cy3dT, the Cy3 fluorescence donor was excited at 515 nm and sensitized fluorescence emission from Cy5 was monitored using a 665 nm long-pass filter (Oriel catalog no. 51330). All slit widths were 1.5–2 mm. The reactant solutions were preformed at 4 °C and then incubated in the reservoir syringes of the stopped-flow instrument at 25 °C for at least 5 min prior to mixing. Longer incubation times had no effect on the results. All concentrations of ssDNA and SSB reported in the text and plotted in Figures 3–5, 7, and 9 are the final concentrations after mixing in the stopped-flow instrument.

Analysis of Kinetic Data. All kinetic time courses that are shown generally represent averages of 10–14 individual traces, except for the very slow time courses (e.g., for the data shown in the inset of Figure 4) where an average of three individual time courses was sufficient. Slow time courses were corrected for slight photobleaching effects when observed. Where applicable, fluorescence time courses were fit to either one or two exponentials using the Applied Photophysics software or MicroMath Scientist Software (Salt Lake City, UT) according to eq 1

$$F(t) = F_{\infty} + \sum_{i=1}^n A_i \exp(-k_{\text{obs},i}t) \quad (1)$$

where $F(t)$ is the fluorescence intensity at time t , F_{∞} is the fluorescence intensity at time ∞ , A_i is the amplitude of the i th relaxation process, $k_{\text{obs},i}$ is the observed rate characterizing the i th relaxation process, and n is the number of relaxation processes. The uncertainties reported for the observed rates ($k_{\text{obs},i}$) represent 68% confidence limits (one standard deviation). Other analyses of the data, including simulations and fitting to the appropriate kinetic or equilibrium models, were performed using MicroMath Scientist Software or Mathematica (Wolfram Research, Champaign, IL).

Scheme 1



THEORETICAL BACKGROUND

Analysis of the Kinetics of DNA Binding and Direct Transfer of SSB. Our data demonstrate that the dominant pathway for dissociation of fluorescently labeled ssDNA (D^*) from its complex with SSB (P) upon addition of a large excess of unlabeled ssDNA (D) occurs via formation of an intermediate in which the SSB tetramer is doubly ligated with DNA (DPD^*) as shown in Scheme 1. The differential equations describing the time dependences of the concentrations of each species in Scheme 1 are given in eqs 2a–d.

$$\frac{d[\text{P}]}{dt} = -(k_1[\text{D}] + k_1^*[\text{D}^*])[\text{P}] + k_{-1}[\text{PD}] + k_{-1}^*[\text{PD}^*] \quad (2a)$$

$$\frac{d[\text{PD}]}{dt} = k_1[\text{D}][\text{P}] - (k_{-1} + k_2^*[\text{D}^*])[\text{PD}] + k_{-2}^*[\text{DPD}^*] \quad (2b)$$

$$\frac{d[\text{PD}^*]}{dt} = k_1^*[\text{D}^*][\text{P}] - (k_{-1}^* + k_2[\text{D}])[\text{PD}^*] + k_{-2}[\text{DPD}^*] \quad (2c)$$

$$\frac{d[\text{DPD}^*]}{dt} = k_2^*[\text{D}^*][\text{PD}] + k_2[\text{D}][\text{PD}^*] - (k_{-2} + k_{-2}^*)[\text{DPD}^*] \quad (2d)$$

Under pseudo-first-order conditions ($[\text{D}]$ and $[\text{D}^*] \gg [\text{P}]$), the concentrations of D and D^* can be treated as constant and the above set of differential equations (eqs 2a–d) reduces to the first-order, linear, homogeneous system of differential equations written below in matrix form as $\dot{\mathbf{P}} = \mathbf{A}\mathbf{P}$

$$\begin{pmatrix} \frac{d[\text{P}]}{dt} \\ \frac{d[\text{PD}]}{dt} \\ \frac{d[\text{PD}^*]}{dt} \\ \frac{d[\text{DPD}^*]}{dt} \end{pmatrix} = \begin{pmatrix} -(k_1[\text{D}] + k_1^*[\text{D}^*]) & k_{-1} & k_{-1}^* & 0 \\ k_1[\text{D}] & -(k_{-1} + k_2^*[\text{D}^*]) & 0 & k_{-2}^* \\ k_1^*[\text{D}^*] & 0 & -(k_{-1}^* + k_2[\text{D}]) & k_{-2} \\ 0 & k_2^*[\text{D}^*] & k_2[\text{D}] & -(k_{-2} + k_{-2}^*) \end{pmatrix} \times \begin{pmatrix} [\text{P}] \\ [\text{PD}] \\ [\text{PD}^*] \\ [\text{DPD}^*] \end{pmatrix} \quad (3)$$

where \mathbf{P} is the vector of concentrations, $\dot{\mathbf{P}}$ is the vector of time derivatives, and \mathbf{A} is the matrix of coefficients. For this

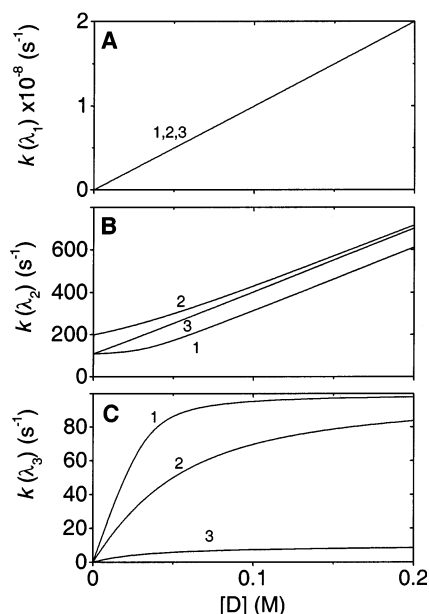


FIGURE 1: Predicted concentration dependences of the three observed rates [$k(\lambda_1)$, $k(\lambda_2)$, and $k(\lambda_3)$] for a direct transfer reaction (Scheme 1) at high concentrations of unlabeled (acceptor) ssDNA. The rate constants and values of $[D]$ used in these simulations set up the condition such that formation of the doubly ligated complex is fast relative to dissociation; i.e., $k_2[D] > k_{-2}$ and k_{-2}^* . The simulations are based on Scheme 1 as described in Theoretical Background using the following parameters: $k_1 = 10^9 \text{ M}^{-1} \text{ s}^{-1}$, $k_1^* = 8 \times 10^8 \text{ M}^{-1} \text{ s}^{-1}$, $k_{-1} = 0.005 \text{ s}^{-1}$, $k_{-1}^* = 0.001 \text{ s}^{-1}$, $k_2 = 3 \times 10^3 \text{ M}^{-1} \text{ s}^{-1}$, $k_2^* = 6 \times 10^3 \text{ M}^{-1} \text{ s}^{-1}$, and $[D^*] = 2 \times 10^{-8} \text{ M}$. Curves 1–3 are simulated for three combinations of the dissociation rate constants from the doubly ligated complex (k_{-2} and k_{-2}^*) as follows: (1) $k_{-2} = 10 \text{ s}^{-1}$ and $k_{-2}^* = 100 \text{ s}^{-1}$, (2) $k_{-2} = 100 \text{ s}^{-1}$ and $k_{-2}^* = 100 \text{ s}^{-1}$, and (3) $k_{-2} = 100 \text{ s}^{-1}$ and $k_{-2}^* = 10 \text{ s}^{-1}$.

system, four eigenvalues (λ_0 , λ_1 , λ_2 , and λ_3) are obtained as the roots of the polynomial equation obtained from the condition $|\mathbf{A} - \lambda\mathbf{I}| = 0$, where \mathbf{I} is the identity matrix. Since one root has the trivial solution $\lambda_0 = 0$, the three eigenvalues (λ_1 – λ_3) will describe the observed rates as a function of the concentration of D (or D^*) for the kinetic pathway shown in Scheme 1.

Values of λ_1 – λ_3 were obtained by solving numerically the polynomial equation obtained from $|\mathbf{A} - \lambda\mathbf{I}| = 0$ for concentrations of unlabeled competitor ssDNA (D) from 10 nM to 0.2 M. The corresponding predicted values of the observed rates [$k(\lambda_1) = -\lambda_1$, $k(\lambda_2) = -\lambda_2$, and $k(\lambda_3) = -\lambda_3$] are plotted in Figures 1 and 2 for conditions of high and low $[D]$, respectively. For these simulations, we fixed the concentration of labeled ssDNA* ($[D^*]$) at $2 \times 10^{-8} \text{ M}$ and used rate constants that are similar to the ones that we have determined experimentally in this work: $k_1 = 10^9 \text{ M}^{-1} \text{ s}^{-1}$, $k_1^* = 8 \times 10^8 \text{ M}^{-1} \text{ s}^{-1}$, $k_{-1} = 0.005 \text{ s}^{-1}$, $k_{-1}^* = 0.001 \text{ s}^{-1}$, $k_2 = 3 \times 10^3 \text{ M}^{-1} \text{ s}^{-1}$, and $k_2^* = 6 \times 10^3 \text{ M}^{-1} \text{ s}^{-1}$. The rate constants for dissociation of one DNA from the doubly ligated complex (k_{-2} and k_{-2}^*) were varied from 10 to 100 s^{-1} . The values of these rate constants are such that binding of the first ssDNA molecule, either labeled or unlabeled (D or D^*), to form a singly ligated complex (PD or PD*) is fast, relative to dissociation ($k_1[D]$ and $k_1^*[D^*] \gg k_{-1}$ and k_{-1}^*), and the rate of formation of the doubly ligated complex (DPD*) is slow compared to the rate of formation of the singly ligated complexes (k_2 and $k_2^* \ll k_1$ and k_1^* , and

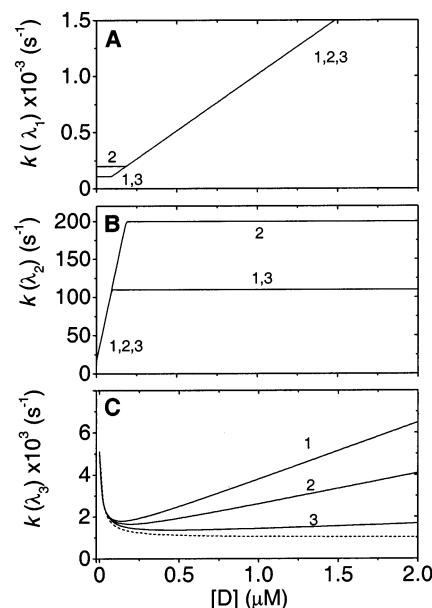


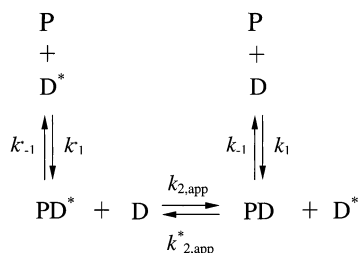
FIGURE 2: Predicted concentration dependences of the three observed rates [$k(\lambda_1)$, $k(\lambda_2)$, and $k(\lambda_3)$] for a direct transfer reaction (Scheme 1) at low concentrations of unlabeled (acceptor) ssDNA (compared to concentrations used in simulations shown in Figure 1). The rate constants and values of $[D]$ used in these simulations set up the condition such that formation of the doubly ligated complex is slow relative to dissociation; i.e., k_{-2} and $k_{-2}^* > k_2[D]$. The simulations are based on Scheme 1 as described in Theoretical Background using the following parameters: $k_1 = 10^9 \text{ M}^{-1} \text{ s}^{-1}$, $k_1^* = 8 \times 10^8 \text{ M}^{-1} \text{ s}^{-1}$, $k_{-1} = 0.005 \text{ s}^{-1}$, $k_{-1}^* = 0.001 \text{ s}^{-1}$, $k_2 = 3 \times 10^3 \text{ M}^{-1} \text{ s}^{-1}$, $k_2^* = 6 \times 10^3 \text{ M}^{-1} \text{ s}^{-1}$, and $[D^*] = 2 \times 10^{-8} \text{ M}$. Curves 1–3 are simulated for three combinations of the dissociation rate constants from the doubly ligated complex (k_{-2} and k_{-2}^*) as follows: (1) $k_{-2} = 10 \text{ s}^{-1}$ and $k_{-2}^* = 100 \text{ s}^{-1}$, (2) $k_{-2} = 100 \text{ s}^{-1}$ and $k_{-2}^* = 100 \text{ s}^{-1}$, and (3) $k_{-2} = 100 \text{ s}^{-1}$ and $k_{-2}^* = 10 \text{ s}^{-1}$.

k_{-2} and $k_{-2}^* \gg k_{-1}$ and k_{-1}^*). These rate constraints apply under the conditions of the experiments reported here.

Figure 1 shows the dependences of the three predicted observed rates on $[D]$ for conditions of high $[D]$ such that $k_2[D] > k_{-2}$ and k_{-2}^* . When $[D] > 0.05 \text{ M}$, where formation of the doubly ligated complex is fast, the dependences of $k(\lambda_1)$ and $k(\lambda_2)$ on $[D]$ are linear (Figure 1A,B) with slopes equal to k_1 and k_2 , respectively. The dependence of $k(\lambda_3)$ on $[D]$ is hyperbolic with plateau values $k(\lambda_3)$ equal to $k_{-2}^* + k_2^*[D^*]$ (Figure 1C). Since in our simulation a $k_2^*[D^*]$ of $1.2 \times 10^{-4} \text{ s}^{-1}$ is very small, the plateau values are determined primarily by k_{-2}^* (10 s^{-1} for curve 3 and 100 s^{-1} for curves 1 and 2).

Figure 2 shows the predicted dependences of the three predicted observed rates on $[D]$ at low $[D]$ such that $k_2[D] \ll k_{-2}$ and k_{-2}^* . In fact, under these conditions, Scheme 1 can be simplified to Scheme 2 (see below). As the concentration of D decreases, the step describing formation of the doubly ligated complex becomes rate-limiting and the behavior of $k(\lambda_2)$ and $k(\lambda_3)$ changes dramatically, whereas $k(\lambda_1)$ is still linearly dependent on $[D]$ with a slope equal to k_1 . The value of $k(\lambda_2)$ is constant over a wide range of ssDNA concentrations (down to 2 – $4 \times 10^{-7} \text{ M}$; see Figure 2B) and is equal to the sum of the dissociation rate constants for dissociation of D and D^* from the doubly ligated complex [$k(\lambda_2) \approx k_{-2} + k_{-2}^*$]. Below a $[D]$ value of $0.2 \mu\text{M}$ (or $0.4 \mu\text{M}$), the magnitude of $k(\lambda_2)$ decreases linearly with $[D]$, with

Scheme 2



a slope also equal to k_1 . The value of $k(\lambda_3)$ (Figure 2C) decreases linearly with decreasing $[\text{D}]$ down to $\sim 0.4 \mu\text{M}$. When $[\text{D}] < 0.4 \mu\text{M}$, $k(\lambda_3)$ starts to increase with decreasing $[\text{D}]$, reaching a value of $\approx 0.005 \text{ s}^{-1}$ at $[\text{D}] = 0$, which corresponds to k_{-1} . The hyperbolic increase in $k(\lambda_3)$ with decreasing $[\text{D}]$ at low $[\text{D}]$ is diagnostic of the competitive binding of D and D^* to P , and will always be observed even in the absence of a direct transfer reaction (i.e., if there were no DPD^* species possible) as indicated by the dashed line in Figure 2C. The linear increase in $k(\lambda_3)$ at high $[\text{D}]$ (solid lines 1–3 in Figure 2C) reflects the formation of the doubly ligated intermediate, DPD^* (i.e., the direct transfer intermediate). An important point which is clear from the simulations in Figure 2C is that the slope of the linear dependence of $k(\lambda_3)$ on $[\text{D}]$ at high $[\text{D}]$ is a sensitive function of the ratio k_{-2}/k_{-2}^* . If $k_{-2} < k_{-2}^*$, the slope is close to the value of k_2 , whereas its value decreases with increasing k_{-2} . Although it appears in Figure 2C that the intercept obtained upon extrapolation of the linear parts of the curves to $[\text{D}] = 0$ is equal to a k_{-1}^* of 0.001 s^{-1} , a more careful inspection of the simulated dependences indicates that both the intercept and the value of $k(\lambda_3)$ at $[\text{D}] = 0$ are functions of $[\text{D}^*]$. This can be readily shown (see below) in analytic form using the simplified Scheme 2.

The stopped-flow experiments reported here monitor the fluorescence changes resulting from dissociation of a fluorescently labeled ssDNA (D^*) from its complex with SSB upon addition of an excess of unlabeled ssDNA (D). When the fluorescent ssDNA is $(\text{dT})_{70}$, the time courses of these fluorescence changes all follow single-exponential functions and the dependence of the observed rate on $[(\text{dT})_{70}]$ displays the behavior shown for $k(\lambda_3)$ in Figure 2C. This suggests that under the conditions of our experiments, $k_2[\text{D}]$ and $k_2^*[\text{D}^*] \ll k_{-2}$ and k_{-2}^* , and thus, we observe only one of the three possible rates corresponding to $k(\lambda_3)$. This also means that under our experimental conditions, the concentration of the doubly ligated intermediate species, DPD^* , is very small and thus the kinetic pathway of Scheme 1 can be simplified to that of Scheme 2. Use of the simpler Scheme 2 results in a reduction from three to two in the number of eigenvalues needed to describe the pathway and also allows us to obtain analytic expressions for these two eigenvalues. Applying the condition $d[\text{PDP}^*]/dt = 0$, we can express $[\text{PDP}^*]$ explicitly using eq 2d and introduce this expression into eqs 2b and 2c to reduce the number of differential equations from four to three as shown in eqs 4a–c

$$\frac{d[\text{P}]}{dt} = -(k_1[\text{D}] + k_1^*[\text{D}^*])[\text{P}] + k_{-1}[\text{PD}] + k_{-1}^*[\text{PD}^*] \quad (4a)$$

$$\frac{d[\text{PD}]}{dt} = k_1[\text{D}][\text{P}] - (k_{-1} + k_{2,\text{app}}^*[\text{D}^*])[\text{PD}] + k_{2,\text{app}}[\text{D}][\text{PD}^*] \quad (4b)$$

$$\frac{d[\text{PD}^*]}{dt} = k_1^*[\text{D}^*][\text{P}] + k_{2,\text{app}}^*[\text{D}^*][\text{PD}] - (k_{-1}^* + k_{2,\text{app}}[\text{D}])[\text{PD}^*] \quad (4c)$$

where $k_{2,\text{app}} = k_2[k_{-2}^*/(k_{-2} + k_{-2}^*)]$ and $k_{2,\text{app}}^* = k_2^*[k_{-2}/(k_{-2} + k_{-2}^*)]$. On the basis of this, the analytic expressions in eqs 5a–d for the two eigenvalues ($\lambda_{1,2}'$ and λ_3') can be found by solving the quadratic equation obtained as before from the condition $|\mathbf{A} - \lambda\mathbf{I}| = 0$, where \mathbf{I} is the identity matrix and \mathbf{A} is the matrix of coefficients corresponding to eqs 4a–c:

$$\lambda_{1,2}' = \frac{-b - \sqrt{b^2 - 4c}}{2} \quad (5a)$$

$$\lambda_3' = \frac{-b + \sqrt{b^2 - 4c}}{2} \quad (5b)$$

where

$$b = (k_1 + k_{2,\text{app}})[\text{D}] + (k_1^* + k_{2,\text{app}}^*[\text{D}^*]) + k_{-1} + k_{-1}^* \quad (5c)$$

$$c = k_{2,\text{app}}[\text{D}](k_1[\text{D}] + k_1^*[\text{D}^*] + k_{-1}) + k_{2,\text{app}}^*[\text{D}^*](k_1[\text{D}] + k_1^*[\text{D}^*] + k_{-1}) + k_{-1}^*k_1[\text{D}] + k_{-1}k_1^*[\text{D}^*] \quad (5d)$$

We note that for the simplified pathway in Scheme 2, the two eigenvalues λ_1 and λ_2 describing Scheme 1 “collapse” into one eigenvalue $\lambda_{1,2}'$ (eq 5a), whereas the second “slow” eigenvalue, λ_3' (eq 5b), corresponds to eigenvalue λ_3 obtained for Scheme 1. These two eigenvalues are related to two theoretical observed rates defined as follows: $k(\lambda_{1,2}') = -\lambda_{1,2}'$ and $k(\lambda_3') = -\lambda_3'$. As discussed above, since we are able to detect only the slowest phase in our experiments, we need to consider only eq 5b. Applying the square-root approximation ($\sqrt{b^2 - 4c} \approx b - 2c/b$ for $2c \ll b^2$) (29) to this equation, we obtain $\lambda_3' \approx -c/b$. Under conditions where k_1 and $k_1^* \gg k_{2,\text{app}}$ and $k_{2,\text{app}}^*$ and $k_1[\text{D}]$ and $k_1^*[\text{D}^*] \gg k_{-1}$ and k_{-1}^* , this reduces to the expression in eq 6.

$$k(\lambda_3') = \frac{k_{-1}^*k_1[\text{D}] + k_{-1}k_1^*[\text{D}^*]}{(k_1[\text{D}] + k_1^*[\text{D}^*])} + k_{2,\text{app}}^*[\text{D}^*] + k_{2,\text{app}}[\text{D}] \quad (6)$$

When $[\text{D}] = 0$, eq 6 reduces to eq 7, which provides an expression for the intercept with the ordinate of the nonlinear region of $k(\lambda_3')$.

$$k(\lambda_3') = k_{-1} + k_{2,\text{app}}^*[\text{D}^*] \quad (7)$$

This intercept, in the limit of $[\text{D}^*] = 0$, yields k_{-1} , the dissociation rate constant for the PD complex.

In the limit of high $[\text{D}]$, eq 6 reduces to eq 8

$$k(\lambda_3') = k_{-1}^* + k_{2,\text{app}}^*[\text{D}^*] + k_{2,\text{app}}[\text{D}] \quad (8)$$

describing the linear dependence of $k(\lambda_3')$ on $[D]$ with a slope equal to $k_{2,app}$ and intercept equal to $(k_{-1}^* + k_{2,app}[D^*])$. Therefore, in the limit of $[D^*] = 0$, the intercept yields k_{-1}^* , the dissociation rate constant for the PD^* complex.

We note that in the absence of a direct transfer pathway such that only a simple competition between D and D^* exists for a single site on the protein (P) (i.e., no doubly ligated species, DPD^* , can form) then only a simple hyperbolic dependence of $k(\lambda_3')$ on $[D]$ will be observed and the values of k_{-1} and k_{-1}^* are given by the values of $k(\lambda_3')$ in the limits of $[D] = 0$ and $[D] \rightarrow \infty$, respectively. A simulated curve for this case is shown as a dashed line in Figure 2C using the following parameters: $k_1 = 10^9 \text{ M}^{-1} \text{ s}^{-1}$, $k_1^* = 8 \times 10^8 \text{ M}^{-1} \text{ s}^{-1}$, $k_{-1} = 0.005 \text{ s}^{-1}$, $k_{-1}^* = 0.001 \text{ s}^{-1}$, and $[D^*] = 2 \times 10^{-8} \text{ M}$.

RESULTS

Equilibrium fluorescence titration studies (17, 28) and isothermal titration calorimetric (ITC) studies (30) have demonstrated that one molecule of $(dT)_{70}$ binds stoichiometrically to one molecule of SSB tetramer over a broad range of solution conditions. In the equilibrium complex, which is favored at monovalent salt concentrations of $\geq 0.2 \text{ M}$, $(dT)_{70}$ wraps around the SSB tetramer interacting with all four SSB subunits. However, the affinity is too high to measure accurately by these techniques except at very high NaBr concentrations ($\geq 1 \text{ M}$). Stopped-flow kinetic studies have shown that the initial binding step is very rapid with an apparent bimolecular association rate constant that is close to diffusion-controlled ($1.1\text{--}1.5 \times 10^9 \text{ M}^{-1} \text{ s}^{-1}$) at low salt concentrations (24). Furthermore, the kinetics of forming the fully wrapped structure are very fast, relative to the time scale for binding. Our previous stopped-flow studies (24) also indicated that the rate constants for dissociation of these complexes are very small ($\ll 1 \text{ s}^{-1}$) and could not be determined accurately from direct mixing experiments. Therefore, to study the dissociation mechanism of SSB–ssDNA complexes in detail, including the possibility of direct transfer of SSB between two ssDNA molecules (20), we designed a series of stopped-flow competition experiments in which an oligo(dT) labeled with fluorescein (F) or Cy3 is prebound to the SSB tetramer and then mixed with a large excess of unlabeled $(dT)_{70}$. Upon formation of a complex of SSB with $F(dT)_{70}$ or $Cy3(dT)_{69}$, a fluorescence quenching or enhancement is observed, respectively. Therefore, dissociation of these oligonucleotides from SSB is accompanied by the corresponding fluorescence change.

In the following studies, we have performed two types of experiments in which the preformed SSB–ssDNA complex is either in the fully wrapped $(SSB)_{65}$ binding mode such that all four subunits are in contact with the ssDNA or in the $(SSB)_{35}$ binding mode in which only two subunits of the SSB tetramer are in contact with the ssDNA. The $(SSB)_{65}$ binding mode is formed from a 1:1 molar ratio of SSB to $(dT)_{70}$. The $(SSB)_{35}$ complex is formed in one of two ways, either a 1:1 molar ratio of SSB to $(dT)_{35}$ or a 2-fold molar excess of SSB bound to $(dT)_{70}$ at low NaCl concentrations for formation of a complex in which two SSB tetramers are bound cooperatively to $(dT)_{70}$ in the $(SSB)_{35}$ binding mode.

Dissociation Kinetics of a Fully Wrapped SSB– $F(dT)_{70}$ Complex. Figure 3 shows a series of stopped-flow traces

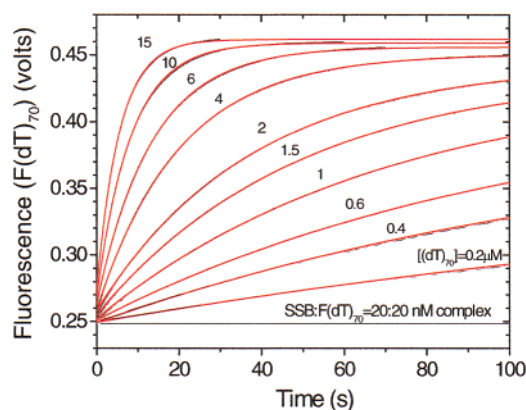


FIGURE 3: Stopped-flow time courses for dissociation of fluorescein-labeled ssDNA $[F(dT)_{70}]$ from a 1:1 SSB complex upon addition of an excess of unlabeled $(dT)_{70}$. Time courses were obtained by monitoring the fluorescein fluorescence under pseudo-first-order conditions after mixing a preformed 1:1 SSB– $F(dT)_{70}$ complex (20 nM each) with increasing amounts of $(dT)_{70}$ (buffer T, pH 8.1, 1 M NaCl, 25 °C). The final concentrations (after mixing) of unlabeled $(dT)_{70}$ used in each experiment are indicated. Each time course was fit to a single-exponential function using eq 1 with $n = 1$ to obtain k_{obs} for each concentration of $(dT)_{70}$. The fits are shown as red lines.

obtained upon mixing a preformed complex (1:1) of SSB and $F(dT)_{70}$ (20 nM) with an excess of unlabeled $(dT)_{70}$ (from 0.2 to 15 μM) in 1 M NaCl (buffer T, pH 8.1, 25 °C). In each case, an enhancement of fluorescein fluorescence is observed, reflecting a net dissociation of $F(dT)_{70}$ from the SSB. Each time course is described well by a single-exponential decay. Values of k_{obs} , obtained by fitting these traces to eq 1 ($n = 1$), increase linearly with increasing $(dT)_{70}$ concentrations as shown in Figure 4A. The slope and intercept determined from a linear least-squares analysis of the data in Figure 4A are $(1.21 \pm 0.01) \times 10^4 \text{ M}^{-1} \text{ s}^{-1}$ and $(2.5 \pm 0.2) \times 10^{-3} \text{ s}^{-1}$, respectively.

For the competition of two ligands (D and D^*) for the same site on a macromolecule P , a hyperbolic dependence of k_{obs} on competitor concentration $[D]$ of the type shown in Figure 2C (dashed line) is expected with limiting values of k_{obs} at $[D] = 0$ and $[D] \rightarrow \infty$ corresponding to dissociation rate constants k_{-1} and k_{-1}^* , respectively. In contrast to that behavior, k_{obs} increases linearly with increasing $[(dT)_{70}]$. Such behavior is indicative of direct binding of the competitor (D) to the SSB– $F(dT)_{70}$ complex (PD^*) in formation of a doubly ligated intermediate (DPD^*). Therefore, we have analyzed these kinetic data according to Scheme 1 (see also Scheme 3). The apparent bimolecular rate constant for forming the DPD^* complex is $(1.21 \pm 0.01) \times 10^4 \text{ M}^{-1} \text{ s}^{-1}$. This rate constant is much lower than the apparent bimolecular rate constant $[k_{1,app} = (2.76 \pm 0.02) \times 10^8 \text{ M}^{-1} \text{ s}^{-1}]$ determined for direct binding of $(dT)_{70}$ to a free SSB tetramer under the same conditions (24).

In principle, three eigenvalues describe the kinetic pathway presented in Scheme 1 (or Scheme 3), and thus, the time courses should display three exponential phases with three observed rates and amplitudes. The fact that only a single exponential phase is observed in our time courses suggests that the two other phases are too fast to be detected under our conditions. For example, the simulations shown in Figure 2 (curves 2) indicate that theoretically predicted values of the first and second observed rates $k(\lambda_1)$ and $k(\lambda_2)$, respec-

Scheme 3

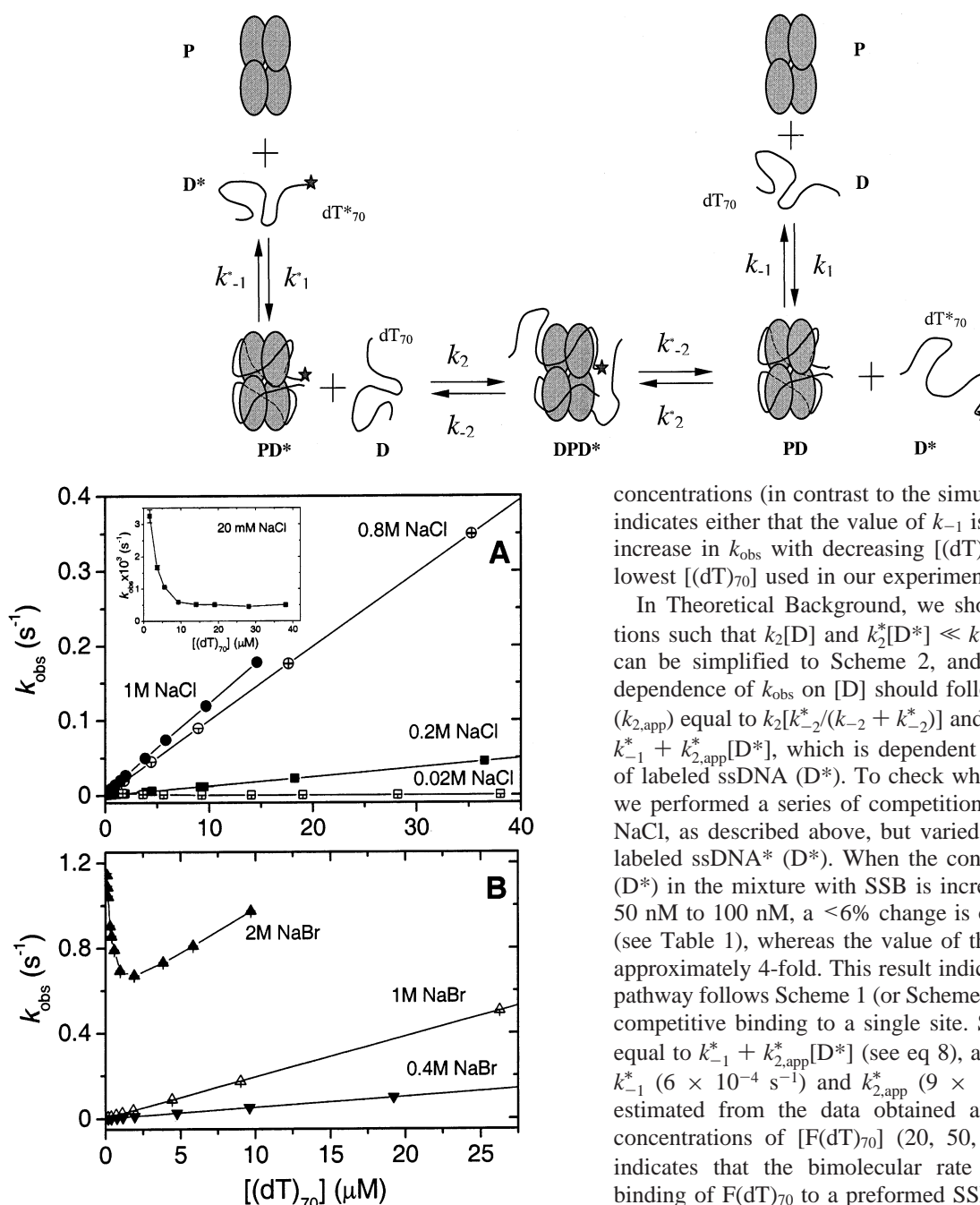


FIGURE 4: Effects of monovalent salt concentration on the dependence on $[(dT)_{70}]$ of the observed rate (k_{obs}) for dissociation of $F(dT)_{70}$ from its 1:1 SSB complex. Stopped-flow experiments of the type described in the legend of Figure 3 were performed, and dissociation was induced by the addition of an excess of unlabeled $(dT)_{70}$ (buffer T, pH 8.1, 25 °C). Values of k_{obs} were determined from single-exponential fits of individual time courses as described in the legend of Figure 3: (A) NaCl and (B) NaBr. The inset shows the dependence of k_{obs} on $[(dT)_{70}]$ in 20 mM NaCl.

tively, are much larger than the value of $k(\lambda_3)$ at 0.2 μM D, which is the lowest DNA competitor concentration used in our experiments. Therefore, it is not surprising that only the slowest observed rate, corresponding to $k(\lambda_3)$, would be observed. Furthermore, since we observe only the linear part of this dependence in our experiments, this indicates that $k_2[D]$ and $k_2^*[D^*] \ll k_{-2}$ and k_{-2}^* under these conditions. The absence of any observable curvature at very low $(dT)_{70}$

concentrations (in contrast to the simulations in Figure 2C) indicates either that the value of k_{-1} is very low or that the increase in k_{obs} with decreasing $[(dT)_{70}]$ occurs below the lowest $[(dT)_{70}]$ used in our experiments.

In Theoretical Background, we show that under conditions such that $k_2[D]$ and $k_2^*[D^*] \ll k_{-2}$ and k_{-2}^* Scheme 1 can be simplified to Scheme 2, and the observed linear dependence of k_{obs} on $[D]$ should follow eq 8 with a slope ($k_{2,\text{app}}$) equal to $k_2[k_{-2}^*/(k_{-2} + k_{-2}^*)]$ and an intercept equal to $k_{-1}^* + k_{2,\text{app}}[D^*]$, which is dependent on the concentration of labeled ssDNA (D^*). To check whether this is the case, we performed a series of competition experiments in 1 M NaCl, as described above, but varied the concentration of labeled ssDNA (D^*). When the concentration of $F(dT)_{70}$ (D^*) in the mixture with SSB is increased from 20 nM to 50 nM to 100 nM, a <6% change is observed in the slope (see Table 1), whereas the value of the intercept increases approximately 4-fold. This result indicates that the reaction pathway follows Scheme 1 (or Scheme 2), rather than simple competitive binding to a single site. Since the intercept is equal to $k_{-1}^* + k_{2,\text{app}}[D^*]$ (see eq 8), approximate values of k_{-1}^* ($6 \times 10^{-4} \text{ s}^{-1}$) and $k_{2,\text{app}}^*$ ($9 \times 10^4 \text{ M}^{-1} \text{ s}^{-1}$) can be estimated from the data obtained at the three different concentrations of $[F(dT)_{70}]$ (20, 50, and 100 nM). This indicates that the bimolecular rate constant ($k_{2,\text{app}}^*$) for binding of $F(dT)_{70}$ to a preformed SSB- $(dT)_{70}$ complex is approximately 9-fold higher than the corresponding value of $k_{2,\text{app}}$ [$(1.20 \pm 0.01) \times 10^4 \text{ M}^{-1} \text{ s}^{-1}$] for the binding of an unlabeled $(dT)_{70}$ to a preformed SSB- $F(dT)_{70}$ complex.

Figure 4 shows the effects of $[\text{NaCl}]$ and $[\text{NaBr}]$ on the dependence of k_{obs} on $[(dT)_{70}]$ for experiments performed by starting with a 1:1 SSB- $F(dT)_{70}$ complex (20 nM each) (buffer T, pH 8.1, 25 °C). Linear dependences are observed at most of the salt concentrations, with the exception of the data obtained in 2 M NaBr and 20 mM NaCl (see the inset in Figure 4A). The slopes and intercepts for the linear parts of each curve (at high D concentrations) are listed in Table 1 (columns 4 and 5). The slope ($k_{2,\text{app}}$) decreases ~10-fold with decreasing NaCl concentrations from 1 to 0.2 M. This is accompanied by a corresponding ~10-fold decrease in the intercept. Therefore, the rate of direct transfer decreases with decreasing salt concentrations. Since $k_{2,\text{app}}$ reflects the rate of formation of the doubly ligated intermediate, this suggests

Table 1: Kinetic Parameters for Binding of SSB to F(dT)₇₀ and (dT)₇₀ and for Binding of (dT)₇₀ to a Preformed (1:1) SSB–F(dT)₇₀ Complex^a

[NaCl] (M)	k_1^b (M ⁻¹ s ⁻¹)	k_1^{*c} (M ⁻¹ s ⁻¹)	$k_{2,app}^d$ (M ⁻¹ s ⁻¹)	$k_{-1}^* + k_{2,app}^*[D^*]^d$ (s ⁻¹)
0.02	$(1.13 \pm 0.03) \times 10^9$	—	—	$\approx 5 \times 10^{-4}$
0.2	$(9.47 \pm 0.30) \times 10^8$	$(8.0 \pm 0.08) \times 10^8$	$(1.20 \pm 0.01) \times 10^3$	$(4.3 \pm 0.3) \times 10^{-4}$
0.2	—	—	$(1.24 \pm 0.01) \times 10^3$	$(2.6 \pm 0.4) \times 10^{-4}$
0.8	—	—	$(9.59 \pm 0.01) \times 10^3$	$(2.2 \pm 0.4) \times 10^{-3}$
1.0	$(2.76 \pm 0.02) \times 10^8$	—	$(1.21 \pm 0.01) \times 10^4$	$(2.5 \pm 0.2) \times 10^{-3}$
1.0	—	—	$(1.17 \pm 0.01) \times 10^4^e$	$(4.4 \pm 0.1) \times 10^{-3}^e$
1.0	—	—	$(1.14 \pm 0.01) \times 10^4^f$	$(9.2 \pm 0.4) \times 10^{-3}^f$
[NaBr] (M)	k_1 (M ⁻¹ s ⁻¹)	k_1^* (M ⁻¹ s ⁻¹)	$k_{2,app}$ (M ⁻¹ s ⁻¹)	$k_{-1}^* + k_{2,app}^*[D^*]$ (s ⁻¹)
0.4	$(3.71 \pm 0.03) \times 10^8$	—	$(5.08 \pm 0.03) \times 10^3$	$(1.35 \pm 0.25) \times 10^{-3}$
1.0	$(1.18 \pm 0.01) \times 10^8$	$(1.40 \pm 0.01) \times 10^8$	$(1.91 \pm 0.01) \times 10^4$	$(3.75 \pm 0.21) \times 10^{-3}$
2.0	$(4.24 \pm 0.01) \times 10^7$	$(5.28 \pm 0.05) \times 10^7$	$(4.11 \pm 0.10) \times 10^4^g$	$(5.72 \pm 0.06) \times 10^{-1}^g$

^a Conditions: buffer T, pH 8.1, 25 °C. ^b Binding experiments were performed under pseudo-first-order conditions: excess of (dT)₇₀ over SSB (from ref 24). ^c Binding experiments were performed under pseudo-first-order conditions: excess of SSB over F(dT)₇₀ (0.2 M NaCl and 1 M NaBr) or excess of F(dT)₇₀ over SSB (2.0 M NaBr). ^d Direct transfer experiments were performed under pseudo-first-order conditions: excess of (dT)₇₀ over the 1:1 F(dT)₇₀–SSB complex [20 nM F(dT)₇₀ and 20 nM SSB]. ^e With 50 nM F(dT)₇₀ and 20 nM SSB. ^f With 100 nM F(dT)₇₀ and 20 nM SSB. ^g With 120 nM F(dT)₇₀ and 20 nM SSB. Rate constants are defined as in Schemes 1 and 2.

that it becomes more difficult to bind the second molecule of (dT)₇₀ to the 1:1 complex at low salt concentrations.

Interestingly, we observe no evidence for direct transfer at the lowest NaCl concentration (20 mM) (see the inset of Figure 4). Instead, after the initial hyperbolic decrease in k_{obs} , a plateau value for k_{obs} of 5×10^{-4} s⁻¹ is observed at > 15 μ M (dT)₇₀. This is the expected behavior for a simple competitive binding between a lower-affinity ligand [(dT)₇₀] and a higher-affinity fluorescent ligand [F(dT)₇₀] for the same site on the SSB. Therefore, under these low-NaCl concentration conditions, we see no evidence for formation of a doubly ligated SSB intermediate.

The behavior of k_{obs} in 2 M NaBr (see Figure 4B) displays both the hyperbolic and linear behavior and corresponds well to the behavior predicted in the simulations in Figure 2C. In the nonlinear region $\{[(dT)_{70}] < 2 \mu\text{M}\}$, the magnitude of k_{obs} decreases from ~ 1.2 to ~ 0.65 s⁻¹ and then increases linearly up to ~ 1 s⁻¹ at 10 μ M (dT)₇₀, with a slope ($k_{2,app}$) of $(4.11 \pm 0.02) \times 10^4$ M⁻¹ s⁻¹ and an intercept ($k_{-1}^* + k_{2,app}^*[D^*]$) of 0.57 ± 0.01 s⁻¹. These values are approximately 8- and 420-fold higher, respectively, than the corresponding values determined in 0.4 M NaBr, which is the lowest concentration of NaBr used in the experiments (see Table 1).

Dissociation Kinetics of a 1:1 SSB–Cy3(dT)₆₉ Complex in 2 M NaBr. The dependences of k_{obs} on [(dT)₇₀] observed for dissociation of F(dT)₇₀ from a 1:1 complex with SSB follow the behavior predicted by Scheme 1. As noted above, data obtained in 2 M NaBr display behavior that is similar to the behavior shown in the simulations in Figure 2C over the entire range of competitor DNA concentrations ([D]) that were used (compare Figures 4B and 2C). To further probe this mechanism, we performed additional experiments at 2 M NaBr by varying the concentration of the fluorescently labeled DNA (D*) used to preform the complex with SSB, since Scheme 1 predicts that this should affect the dependence of k_{obs} on [D].

These direct transfer experiments were performed using ssDNA labeled with a different fluorophore, Cy3. The Cy3(dT)₆₉ (20, 50, or 100 nM) was pre-equilibrated with SSB (20 nM) before mixing in the stopped-flow instrument with a large excess of unlabeled (dT)₇₀ in 2 M NaBr (buffer

T, pH 8.1, 25 °C). When Cy3(dT)₆₉ binds to SSB, its Cy3 fluorescence is enhanced (24), and thus, we observe a decrease in the Cy3 fluorescence upon dissociation of Cy3(dT)₆₉ from SSB. A series of time courses from one set of experiments is shown in Figure 5A. All of the resulting time courses are described well by single-exponential decreases in Cy3 fluorescence, with no evidence for multi-exponential behavior. The resulting plots of k_{obs} versus [(dT)₇₀] for the three concentrations of Cy3(dT)₆₉ are shown in Figure 5B. Each data set shows a dependence on [(dT)₇₀] (D) that is similar in shape to that obtained with the F(dT)₇₀ DNA in 2 M NaBr (see Figure 4B) and to the behavior predicted for Scheme 1 (see Figure 2C). The slopes at high (dT)₇₀ concentrations are the same for each set of data with an average $k_{2,app}$ value of $(3.53 \pm 0.28) \times 10^4$ M⁻¹ s⁻¹, which is close to the $k_{2,app}$ value of $(4.11 \pm 0.10) \times 10^4$ M⁻¹ s⁻¹ obtained with the F(dT)₇₀ DNA. The corresponding intercepts obtained upon linear extrapolation of the data obtained at high (dT)₇₀ concentrations to 0 M (dT)₇₀ increase with increasing [Cy3(dT)₆₉] from 0.32 to 0.41 s⁻¹, as predicted by eq 8. From these data and eq 8 (intercept = $k_{-1}^* + k_{2,app}^*[D^*]$), we calculate a k_{-1}^* of 0.30 s⁻¹ and a $k_{2,app}^*$ of 10.8×10^5 M⁻¹ s⁻¹ in 2 M NaBr, which are 500- and 12-fold higher, respectively, than the corresponding values in 1 M NaCl.

Lower uncertainties in the estimates of all of the rate constants in Scheme 2 were obtained upon performing a global nonlinear least-squares fitting of all three sets of data in Figure 5B using eq 5b. This was done in two ways, either by constraining the values of k_1 and k_1^* to their values obtained in independent experiments ($k_1 = 4.2 \times 10^7$ M⁻¹ s⁻¹ and $k_1^* = 8.2 \times 10^7$ M⁻¹ s⁻¹) or by letting all six rate constants float independently. The resulting rate constants are given in Table 2 (columns 3 and 4, respectively) and indicate that constraining the values of k_1 and k_1^* had no effect on the values of the other rate constants within our uncertainties. From this analysis, we obtain a k_{-1}^* of 0.029 ± 0.01 s⁻¹ and a k_{-1} of 1.9 ± 0.3 s⁻¹ as the rate constants for dissociation of Cy3(dT)₆₉ and (dT)₇₀, respectively, from their 1:1 complexes with SSB. The latter value agrees well with the k_{-1} of 1.60 ± 0.03 s⁻¹ obtained from our previous direct mixing experiments (24).

Table 2: Kinetic Parameters for Direct Association of SSB with Cy3(dT)₆₉ and (dT)₇₀ and for Binding of (dT)₇₀ to a Prebound SSB–Cy3(dT)₆₉ Complex in 2 M NaBr^a

	direct mixing experiments ^b	competition experiments ^c	
k_1 (M ⁻¹ s ⁻¹)	$(4.2 \pm 0.1) \times 10^7$	4.2×10^7 (fixed)	$(2.5 \pm 0.9) \times 10^7$
k_{-1} (s ⁻¹)	1.60 ± 0.03	1.92 ± 0.04	1.94 ± 0.31
k_1^* (M ⁻¹ s ⁻¹)	$(8.2 \pm 0.1) \times 10^7$	8.2×10^7 (fixed)	$(5.4 \pm 1.5) \times 10^7$
	$(8.4 \pm 0.4) \times 10^7$		
k_{-1}^* (s ⁻¹)	—	0.29 ± 0.01	0.29 ± 0.01
$k_{2,app}$ (M ⁻¹ s ⁻¹)	—	$(3.6 \pm 0.1) \times 10^4$	$(3.7 \pm 0.2) \times 10^4$
$k_{2,app}^*$ (M ⁻¹ s ⁻¹)	—	$(8.1 \pm 1.3) \times 10^5$	$(6.7 \pm 1.7) \times 10^5$

^a Conditions: buffer T, pH 8.1, 25 °C. ^b Binding experiments were performed under pseudo-first-order conditions [data for (dT)₇₀ from ref 24]. ^c Competition experiments performed under pseudo-first-order conditions: excess of (dT)₇₀ over the Cy3(dT)₆₉–SSB complex (see Figure 5). Data were fitted simultaneously to eq 5b with k_1 and k_2 fixed according to values obtained in direct mixing experiments (column 3) or by floating all parameters (column 4). Rate constants are defined as in Schemes 1 and 2.

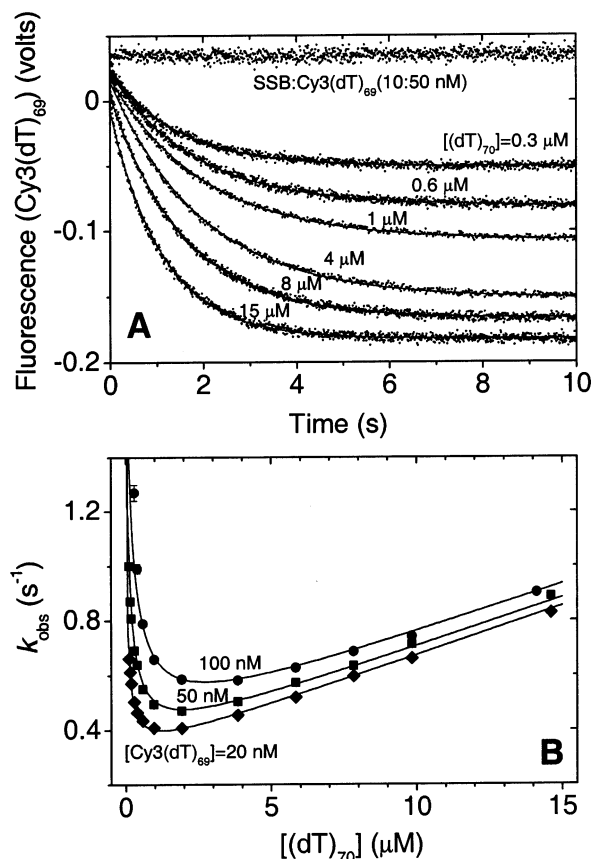


FIGURE 5: Kinetics of dissociation of Cy3(dT)₆₉ from a 1:1 complex with SSB upon addition of an excess of (dT)₇₀. (A) Cy3(dT)₆₉ fluorescence time courses were obtained by mixing a preformed SSB–Cy3(dT)₆₉ complex (20 and 50 nM, respectively) with varying concentrations of (dT)₇₀ in the stopped-flow apparatus (2 M NaBr, buffer T, pH 8.1, 25 °C). The final concentrations of (dT)₇₀ are indicated above each trace. Solid lines are the best fits of the time courses to single-exponential functions using eq 1 (with $n = 1$) from which values of k_{obs} were obtained. (B) Values of k_{obs} plotted as a function of [(dT)₇₀] were determined from experiments in which the concentration of Cy3(dT)₆₉ in the preincubated complex with SSB was varied: (◆) 20 nM SSB and 20 nM Cy3(dT)₆₉, (■) 20 nM SSB and 50 nM Cy3(dT)₆₉, and (●) 20 nM SSB and 100 nM Cy3(dT)₆₉. Solid curves are simulations based on the best fit parameters resulting from a global fit of all three data sets to eq 5b (Scheme 2): $k_{-1}^* = 0.29 \pm 0.01$ s⁻¹, $k_{-1} = 1.92 \pm 0.04$ s⁻¹, $k_{2,app} = (3.6 \pm 0.1) \times 10^4$ M⁻¹ s⁻¹, and $k_{2,app}^* = (8.1 \pm 1.3) \times 10^5$ M⁻¹ s⁻¹ if $k_1 = 4.2 \times 10^7$ M⁻¹ s⁻¹ and $k_1^* = 8.2 \times 10^7$ M⁻¹ s⁻¹.

This global analysis also yields a $k_{2,app}$ of $(3.6 \pm 0.1) \times 10^4$ M⁻¹ s⁻¹ and a $k_{2,app}^*$ of $(8.1 \pm 1.3) \times 10^5$ M⁻¹ s⁻¹, the apparent rate constants for the binding of (dT)₇₀ to an SSB–

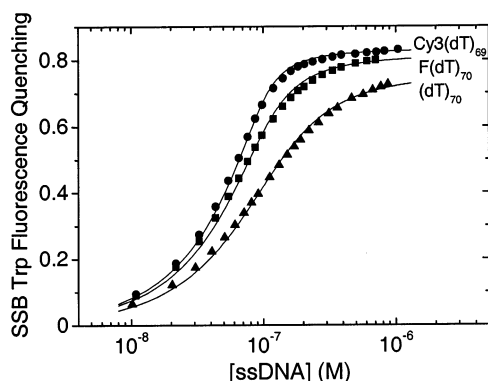
Cy3(dT)₆₉ complex and for the binding of Cy3(dT)₆₉ to an SSB–(dT)₇₀ complex, respectively (see Scheme 2). Although these differ significantly ($k_{2,app}^*/k_{2,app} \approx 22$), recall that both of these apparent rate constants are actually defined as follows: $k_{2,app} = k_2[k_{-2}/(k_{-2} + k_{-2}^*)]$ and $k_{2,app}^* = k_2^*[k_{-2}/(k_{-2} + k_{-2}^*)]$ (see Theoretical Background). In fact, we could resolve the actual values of k_2^* and k_2 if estimates of k_{-2} and k_{-2}^* (see Scheme 1) were available. However, values of these dissociation rate constants could not be determined directly from our studies since the reactions are too fast. Nevertheless, if we assume that the ratio of k_{-2}/k_{-2}^* is the same as the ratio of k_{-1}/k_{-1}^* (1.9 s⁻¹/ 0.29 s⁻¹ ≈ 6) (see Table 2), we predict that $k_2 = 2.5 \times 10^5$ M⁻¹ s⁻¹ and $k_2^* = 9.5 \times 10^5$ M⁻¹ s⁻¹. Thus, these two bimolecular rate constants may differ by a factor of as little as 4, which is quite similar to that observed for the ratio of k_1^*/k_1 , which is 2.

Comparison of Kinetic and Equilibrium Studies of the Binding of Cy3(dT)₆₉ and F(dT)₇₀ to the SSB Tetramer. In our previous stopped-flow studies, we have shown that in 1.0 M NaCl (buffer T, pH 8.1, 25.0 °C), the kinetics of formation of a fully wrapped 1:1 complex of SSB are identical regardless of whether we used unlabeled (dT)₇₀ or the doubly labeled Cy5(dT)₆₅Cy3dT (24). This suggests that there is little influence of the fluorescent probes attached to the ssDNA under these conditions. However, in the study presented here, we find that the apparent bimolecular rate constants obtained at high NaBr concentrations are more sensitive to whether the ssDNA contains a fluorescent label. Stopped-flow experiments monitoring either the SSB Trp fluorescence or the F/Cy3 fluorescence of the ssDNA* indicate that the apparent bimolecular rate constants, k_1^* , are slightly higher than the corresponding values of k_1 determined for unlabeled (dT)₇₀ (see Tables 1 and 2). The largest difference is observed in 2 M NaBr where $k_1 = (4.2 \pm 0.1) \times 10^7$ M⁻¹ s⁻¹ for (dT)₇₀, $k_1^* = (5.3 \pm 0.1) \times 10^7$ M⁻¹ s⁻¹ for F(dT)₇₀, and $k_1^* = (8.2 \pm 0.1) \times 10^7$ M⁻¹ s⁻¹ for Cy3(dT)₆₉. The negative intercepts observed in each of these experiments indicate that $k_1^*[\text{ssDNA}^*] \gg k_{-1}^*$, making it difficult to obtain a reliable estimate of k_{-1}^* based solely on these experiments (24).

As opposed to titrations performed in NaCl, those performed in buffers containing high NaBr concentrations can be used to obtain accurate estimates of equilibrium binding constants (K_{obs}) for the SSB–(dT)₇₀ interaction. Binding isotherms obtained by titrating SSB (0.1 μM) with (dT)₇₀,

Table 3: Kinetic and Equilibrium Data for (dT)₇₀, F(dT)₇₀, and Cy3(dT)₆₉ Binding to SSB in the Presence of 2 M NaBr To Form a Fully Wrapped (SSB)₆₅ Complex^a

ssDNA	K_{obs} (M ⁻¹) equilibrium titration	k_1/k_{-1} (M ⁻¹)	k_1 (M ⁻¹ s ⁻¹)	k_{-1} (s ⁻¹)
dT ₇₀ ^b	$(2.7 \pm 0.1) \times 10^7$	$(2.6 \pm 0.1) \times 10^7$	$(4.2 \pm 0.1) \times 10^7$	1.60 ± 0.03
FdT ₇₀	$(8.6 \pm 0.7) \times 10^7$	$\geq (9.2 \pm 0.1) \times 10^7$	$(5.3 \pm 0.1) \times 10^7$	$\leq 0.57 \pm 0.01$
Cy3dT ₆₉	$(2.1 \pm 0.2) \times 10^8$	$(2.8 \pm 0.1) \times 10^8$	$(8.2 \pm 0.1) \times 10^7$	0.29 ± 0.01

^a Conditions: buffer T, pH 8.1, 25 °C. ^b Data from ref 24.FIGURE 6: Equilibrium isotherms for the SSB tetramer (0.1 μM) binding to (dT)₇₀ (▲), F(dT)₇₀ (■), and Cy3(dT)₆₉ (●) performed by monitoring the quenching of SSB Trp fluorescence (buffer T, pH 8.1, 2 M NaBr, 25 °C). The solid lines are the best fits to a single-site binding model with the fitting parameters listed in Table 3.

F(dT)₇₀, or Cy3(dT)₆₉ and monitoring SSB Trp fluorescence are shown in Figure 6 (buffer T, pH 8.1, 2 M NaBr, 25 °C). These titrations indicate that SSB binds with highest affinity to Cy3(dT)₆₉ and lowest affinity to (dT)₇₀. The values of K_{obs} obtained by fitting these isotherms to a 1:1 binding model are listed in Table 3. It is interesting to compare these equilibrium constants with the values of k_1/k_{-1} determined from our stopped-flow kinetic experiments with (dT)₇₀, F(dT)₇₀, and Cy3(dT)₆₉ under the same conditions (see Tables 1 and 2). The ratios, k_1/k_{-1} , are also presented in Table 3 and agree well with the values of K_{obs} . Both of these results indicate that in 2 M NaBr the affinity of SSB for (dT)₇₀ increases approximately 3- and 10-fold, respectively, upon incorporation of fluorescein and Cy3 at the 5'-end of the ssDNA, indicating that these dyes are involved in direct interactions with the protein.

Dissociation Kinetics of 1:1 Complexes of F(dT)₃₅ Bound to an SSB Tetramer. To determine whether the availability of free DNA binding sites on the SSB tetramer influences the kinetics of dissociation of a prebound ssDNA, we performed experiments with a shorter oligonucleotide, (dT)₃₅. An SSB tetramer can bind two molecules of (dT)₃₅ at saturation, and on average, each (dT)₃₅ interacts with only two SSB subunits. Furthermore, the first (dT)₃₅ molecule binds with much higher affinity than the second, reflecting significant negative cooperativity, which is also dependent on salt concentration and type (17, 30, 31). Therefore, a second ssDNA binding site will be unoccupied in a preformed 1:1 complex of SSB bound to (dT)₃₅. To better compare these experiments with those performed with F(dT)₇₀–SSB complexes, we used (dT)₃₅ labeled with fluorescein [F(dT)₃₅]. In a 1:1 complex with SSB, the F(dT)₃₅ is bound stoichiometrically, thus leaving two unoccupied subunits available for the binding of a second (dT)₃₅

molecule. As was observed with F(dT)₇₀, the time courses for dissociation of F(dT)₃₅ from SSB upon addition of excess (dT)₃₅ (see Figure 7) are described well by Scheme 1 (see also Scheme 4). However, as we discuss below, for the F(dT)₃₅ experiments, we now observe that the rate-limiting step in the direct transfer process is the rate of dissociation of F(dT)₃₅ from the doubly ligated SSB tetramer, indicating that $k_{-2}^* < k_2[\text{D}]$. This behavior is clearly different from that which was observed for the (dT)₇₀ kinetics, where we found that the direct transfer rate was limited by the binding of the second molecule of (dT)₇₀ ($k_2[\text{D}]$ and $k_2^*[\text{D}^*] \ll k_{-2}$ and k_{-2}^*).

Figure 7A shows kinetic time courses for dissociation of F(dT)₃₅ from a 1:1 complex with SSB (20 and 20 nM) upon addition of an excess of unlabeled (dT)₃₅ in 0.4 M NaBr (buffer T, pH 8.1, 25 °C). In contrast to what was observed with the longer (dT)₇₀, the time courses exhibit two exponential phases, indicating that at least two steps are needed to describe the dissociation of F(dT)₃₅. These time courses were fit to a double-exponential function (eq 1 with $n = 2$) to obtain the observed rates, $k_{\text{obs},1}$ and $k_{\text{obs},2}$, which are plotted as a function of [(dT)₃₅] in panels B and C of Figure 7, respectively. The observed rate for the fast phase ($k_{\text{obs},1}$) increases linearly with [(dT)₃₅], with a slope of $(2.56 \pm 0.07) \times 10^7 \text{ M}^{-1} \text{ s}^{-1}$ and an intercept of $8.55 \pm 0.39 \text{ s}^{-1}$. However, the rate for the slower phase ($k_{\text{obs},2}$) increases hyperbolically with increasing (dT)₃₅ concentrations, reaching a plateau value of $\sim 1.5\text{--}1.6 \text{ s}^{-1}$ at $> 2 \mu\text{M}$ (dT)₃₅. The behavior shown in panels B and C of Figure 7 is qualitatively similar to the simulated behavior of the theoretical rates $k(\lambda_2)$ and $k(\lambda_3)$ shown in panels B and C of Figure 1. Therefore, on the basis of Scheme 1 (see also Scheme 3), we ascribe the fast phase to the formation of the doubly ligated D*PD intermediate, characterized by the bimolecular rate constant k_2 , given by the slope of the linear dependence of $k_{\text{obs},1}$ on [(dT)₃₅]. Then the hyperbolic dependence of $k_{\text{obs},2}$ reflects dissociation of D* from the D*PD complex, and the plateau value is given by $k_{-2}^* + k_2^*[\text{D}^*]$. A rough estimate of the contribution from the $k_2^*[\text{D}^*]$ term can be obtained by assuming that $k_2^* \approx k_2 = 3 \times 10^7 \text{ M}^{-1} \text{ s}^{-1}$. Then at 20 nM F(dT)₃₅, we estimate $k_2^*[\text{F(dT)}_{35}] = 0.6 \text{ s}^{-1}$, from which we estimate $k_{-2} \approx 1 \text{ s}^{-1}$.

Similar experiments examining the kinetics of transfer of SSB from F(dT)₃₅ to (dT)₃₅ were also performed at 20 mM and 0.2 M NaCl, and the results are summarized in Table 4. As was observed in 0.4 M NaBr, the time courses can be described by two exponential phases, although in 20 mM and 0.2 M NaCl there was an indication that a third low-amplitude phase (contributing up to $\sim 15\%$ to the total amplitude) is also present. We ascribe the third phase to the fact that at these NaCl concentrations a small population of complexes can form in which one SSB tetramer has two molecules of F(dT)₃₅ bound (D*PD* complex), in addition

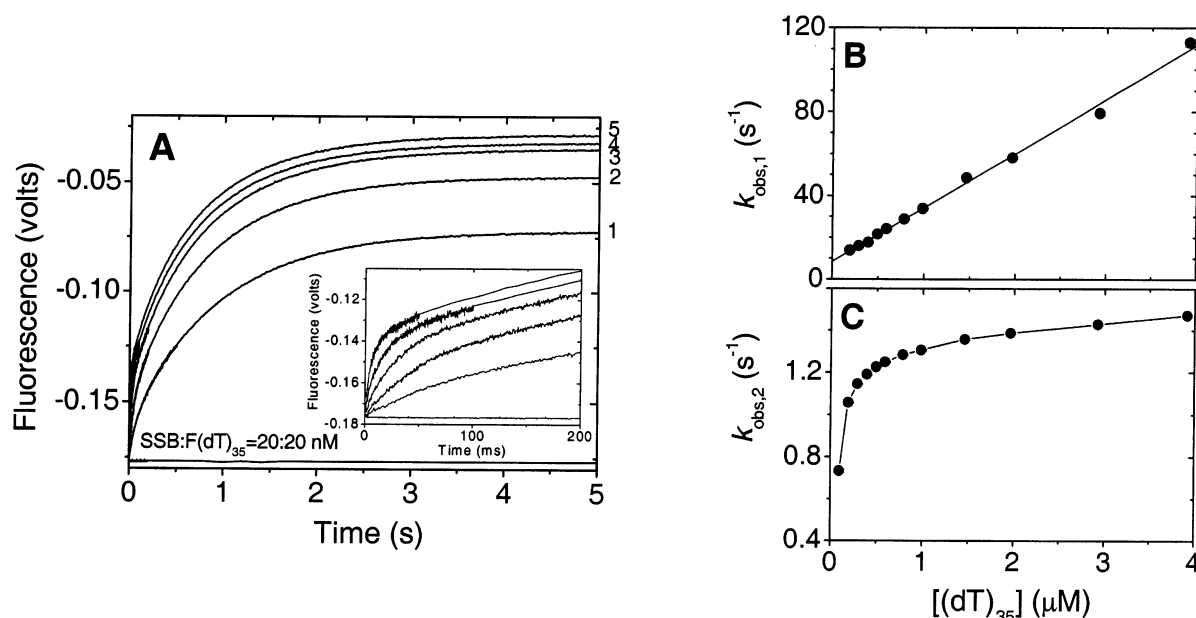
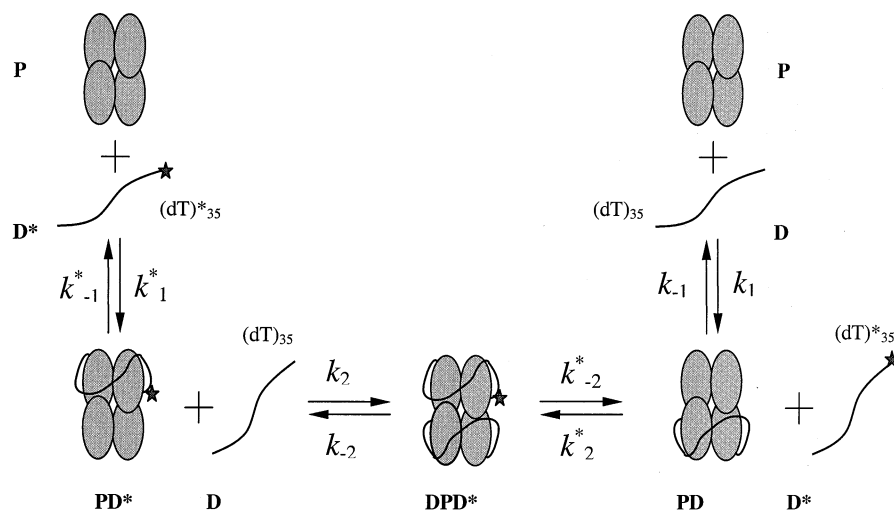


FIGURE 7: Kinetics of F(dT)₃₅ release from a 1:1 complex with SSB (0.4 M NaBr, buffer T, pH 8.1, 25 °C). (A) Time courses were obtained by monitoring fluorescein (F) fluorescence enhancement upon mixing a preformed 1:1 SSB–F(dT)₃₅ (20 and 20 nM, respectively) with the following final concentrations of (dT)₃₅ after mixing: (1) 0.19, (2) 0.49, (3) 0.98, (4) 1.96, and (5) 3.92 μM. Each time course is biphasic with a fast phase that is distinguishable when plotted on a 200 ms time scale (see the inset). (B and C) Observed rates $k_{\text{obs},1}$ and $k_{\text{obs},2}$, respectively, obtained from fitting each time course to a double-exponential function using eq 1 (with $n = 2$) plotted as a function of [(dT)₃₅]. The parameters obtained from a linear least-squares fit of the data in panel B are $8.55 \pm 0.39 \text{ s}^{-1}$ (intercept) and $(2.56 \pm 0.07) \times 10^7 \text{ M}^{-1} \text{ s}^{-1}$ (slope).

Scheme 4



to the PD* complex which is the major species formed. Hence, we also observe dissociation of F(dT)₃₅ from the D*PD* complex as a third phase. This third phase may also be present in the time courses performed at 0.4 M NaBr; however, its amplitude is sufficiently low that it is undetectable. We do not believe that this third phase is relevant to the direct transfer kinetics, and thus, we have not considered it further.

For the data obtained in 20 mM NaCl, the observed rates for the fast phase increase linearly with [(dT)₃₅] with a slope k_2 of $2.2\text{--}3.3 \times 10^6 \text{ M}^{-1} \text{ s}^{-1}$ and an intercept of $4.2\text{--}4.8 \text{ s}^{-1}$. The rate constant for the slower phase is a hyperbolic function of [(dT)₃₅] with a plateau value of $\sim 0.3 \text{ s}^{-1}$. Analysis of the data in 0.2 M NaCl gives a corresponding k_2 value of $(6.3 \pm 0.1) \times 10^6 \text{ M}^{-1} \text{ s}^{-1}$ and an intercept of $\sim 2.1 \pm 0.5 \text{ s}^{-1}$ for the fast phase [over the (dT)₃₅ concentration range

Table 4: Kinetics of (dT)₃₅ Binding to a Preformed 1:1 SSB–F(dT)₃₅ Complex^a

salt	first phase (linear)		second phase (hyperbolic)
	k_2 (M ⁻¹ s ⁻¹)	intercept (s ⁻¹)	$k_{-2}^* + k_2^*[\text{D}^*]$ (s ⁻¹)
0.02 M NaCl ^b	$(3.3 \pm 0.9) \times 10^6$	4.2 ± 0.2	~ 0.3
	$(2.2 \pm 0.1) \times 10^6$	4.8 ± 0.2	~ 0.3
0.2 M NaCl	$> 6.3 \times 10^7$	2.1 ± 0.5	~ 0.1
0.4 M NaBr	$(2.6 \pm 0.1) \times 10^7$	8.6 ± 0.4	~ 1.6

^a Conditions: buffer T, pH 8.1, 25 °C. Binding experiments were performed under pseudo-first-order conditions: excess of (dT)₃₅ over the SSB–F(dT)₃₅ complex (20 and 20 nM, respectively). ^b The results of two sets of experiments are listed. Rate constants are defined as in Scheme 1.

of $0.2\text{--}0.8 \mu\text{M}$). The observed rate for the slower phase does not exceed $\sim 0.1 \text{ s}^{-1}$. On the basis of these data and the data

obtained in 0.4 M NaBr, we conclude that the formation of the D*PD complex with (dT)₃₅ is fast ($k_2 = 2.2 \times 10^6$ to $6.3 \times 10^7 \text{ M}^{-1} \text{ s}^{-1}$) and that the rate-limiting step is dissociation of D* [F(dT)₃₅] from the D*PD complex, occurring with a rate constant ranging from 0.1 to 1.6 s^{-1} (see Schemes 1 and 3). This indicates that although the overall rate of direct transfer is faster for SSB bound to the shorter (dT)₃₅, the rate-limiting step for direct transfer is not the rate of formation of the doubly ligated complex, as is the case with (dT)₇₀, but rather the rate of dissociation of the fluorescently labeled ssDNA* from this complex. This presumably reflects the fact that there is an available ssDNA binding site on the 1:1 SSB–(dT)₃₅ complex to which a second ssDNA molecule can rapidly bind.

We note that as opposed to the experiments performed in 0.4 M NaBr and 20 mM NaCl, the dependence of $k_{\text{obs},1}$ on [(dT)₃₅] in 0.2 M NaCl (data not shown) is not linear over the entire range of competitor concentrations and starts to deviate toward lower values above $\sim 1 \mu\text{M}$ (dT)₃₅. The fit of this dependence of $k_{\text{obs},1}$ on [(dT)₃₅] to a hyperbola predicts a plateau value at approximately 280 s^{-1} . This behavior may provide evidence for an additional step in Scheme 1 following formation of the doubly ligated complex (DPD*), prior to the release of D*. In any case, the slope [$(6.3 \pm 0.1) \times 10^7 \text{ M}^{-1} \text{ s}^{-1}$] of the initial part of the hyperbolic dependence still provides a lower limit for the bimolecular rate constant for the binding of D to the PD* complex. In fact, in previous stopped-flow studies of (dT)₃₅ binding to SSB performed under the same conditions (24), we determined a bimolecular rate constant for binding of the second (dT)₃₅ molecule to the SSB tetramer of $(1.03 \pm 0.04) \times 10^8 \text{ M}^{-1} \text{ s}^{-1}$ by monitoring quenching of the SSB Trp fluorescence. This is within a factor of 2 of the value we obtain from the slope of the linear part of the plot of $k_{\text{obs},1}$ versus [(dT)₃₅]. Therefore, in Table 3 the value of k_2 in 0.2 M NaCl is listed as $>6.3 \times 10^7 \text{ M}^{-1} \text{ s}^{-1}$.

Kinetics of Direct Transfer of SSB Tetramers Bound Cooperatively in the (SSB)₃₅ Binding Mode. All of the experiments discussed above start with complexes in which a single SSB tetramer is prebound to an oligodeoxynucleotide in a 1:1 complex. However, at low salt concentrations, SSB tetramers can bind with positive “unlimited” cooperativity to long ssDNA (≥ 70 nucleotides) in the so-called (SSB)₃₅ binding mode (3, 10, 11). On the basis of studies of SSB binding to (dA)₇₀, a nearest neighbor unlimited cooperativity parameter, ω , has been estimated to be $\sim 10^5$ (buffer T, pH 8.1, 125 mM NaCl, 25.0 °C) (12). We therefore sought to determine if the kinetics of SSB transfer were influenced if two SSB tetramers were bound cooperatively to the same molecule of (dT)₇₀ in the preformed complex.

In the (SSB)₃₅ binding mode, ssDNA interacts with an average of two subunits of the tetramer (7, 8, 31). Equilibrium ITC and analytical ultracentrifugation experiments performed with (dT)₇₀ at $\leq 20 \text{ mM}$ NaCl (A. G. Kozlov and T. M. Lohman, unpublished results) indicate that binding of (dT)₇₀ to SSB is much stronger than to (dA)₇₀, and at high binding densities, the only complexes observed are those in which two SSB tetramers are bound to a single molecule of (dT)₇₀. However, upon titration with additional (dT)₇₀, dissociation of the cooperative complex occurs, accompanied by the formation of fully wrapped 1:1 SSB–(dT)₇₀ complexes.

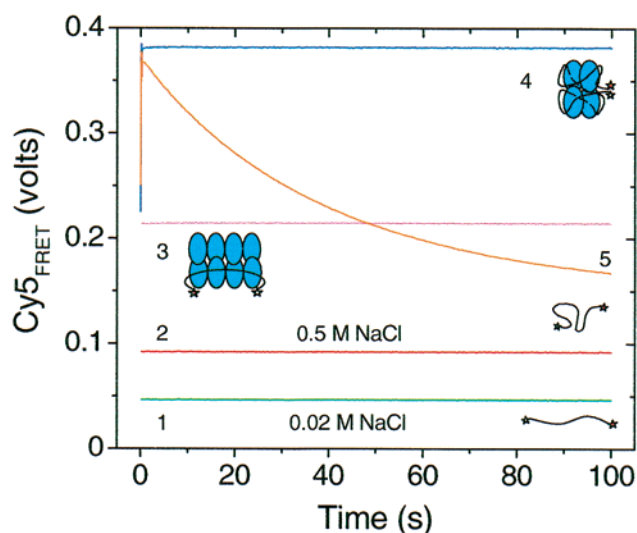


FIGURE 8: Cy5 FRET levels for Cy5(dT)₆₅Cy3dT and its various complexes with SSB: curve 1 (green), Cy5 FRET for free Cy5(dT)₆₅Cy3dT (10 nM) in 20 mM NaCl; curve 2 (red), Cy5 FRET for free Cy5(dT)₆₅Cy3dT (10 nM) in 0.5 M NaCl; curve 3 (magenta), Cy5 FRET for Cy5(dT)₆₅Cy3dT (10 nM) in an (SSB)₃₅ complex with SSB (40 nM) [two SSB tetramers bound per Cy5(dT)₆₅Cy3dT]; curve 4 (blue), time course showing the rapid transition (increase in Cy5 FRET within 100 ms) from the 2:1 (SSB)₃₅ complex (40 nM SSB and 10 nM DNA) in 20 mM NaCl to the (SSB)₆₅ complex induced by the addition of NaCl to a final concentration of 0.5 M; and curve 5 (orange), time course showing the rapid transition (increase in Cy5 FRET within 100 ms) from the 2:1 (SSB)₃₅ complex (40 nM SSB and 10 nM DNA) in 20 mM NaCl to the (SSB)₆₅ complex followed by the much slower decrease in Cy5 FRET reflecting dissociation of Cy5(dT)₆₅Cy3dT from its (SSB)₆₅ complex into solution upon addition of an excess of (dT)₇₀ (final concentration of $5 \mu\text{M}$) along with an increase in the NaCl concentration. All experiments were performed in buffer T at pH 8.1 and 25 °C.

For our kinetics experiments, we prebound two SSB tetramers to Cy5(dT)₆₅Cy3dT, which is labeled with the Cy3/Cy5 FRET pair such that Cy5 is at the 5'-end and Cy3 is at the 3'-end. We used this DNA since the Cy5 FRET signal obtained by exciting the Cy3 donor and monitoring the Cy5 acceptor fluorescence differs significantly when the SSB is bound in the fully wrapped (SSB)₆₅ mode (1:1 complex) versus when two SSB tetramers are bound in a 2:1 complex in the (SSB)₃₅ mode versus when the ssDNA is free as shown in Figure 8. Line 1 in Figure 8 shows the Cy5 (acceptor) FRET signal of the free DNA (10 nM) in 20 mM NaCl. Upon addition of 40 nM SSB to the 10 nM DNA, a 2:1 (SSB)₃₅ complex is formed with an approximately 4-fold increase in the magnitude of the Cy5 FRET signal (line 3), suggesting that the two ends of the DNA within this complex are closer together on average than in the free DNA. When [NaCl] is increased from 20 mM to 0.5 M, the SSB–ssDNA complex undergoes a transition to the fully wrapped 1:1 (SSB)₆₅ complex, which has an even higher-magnitude Cy5 FRET signal (line 4) due to the fact that the two ends of the Cy5(dT)₆₅Cy3dT DNA are closer together in this complex (18, 24). As shown in Figure 8, this transition from the 2:1 (SSB)₃₅ complex to the 1:1 (SSB)₆₅ complex occurs within ~ 100 ms. It is interesting to note that the FRET signal of the free ssDNA [Cy5(dT)₆₅Cy3dT] is also sensitive to the salt concentration, increasing approximately 2-fold as [NaCl] increases from 20 mM to 0.5 M (lines 1 and 2 in Figure 8, respectively). This reflects the fact that the average distance

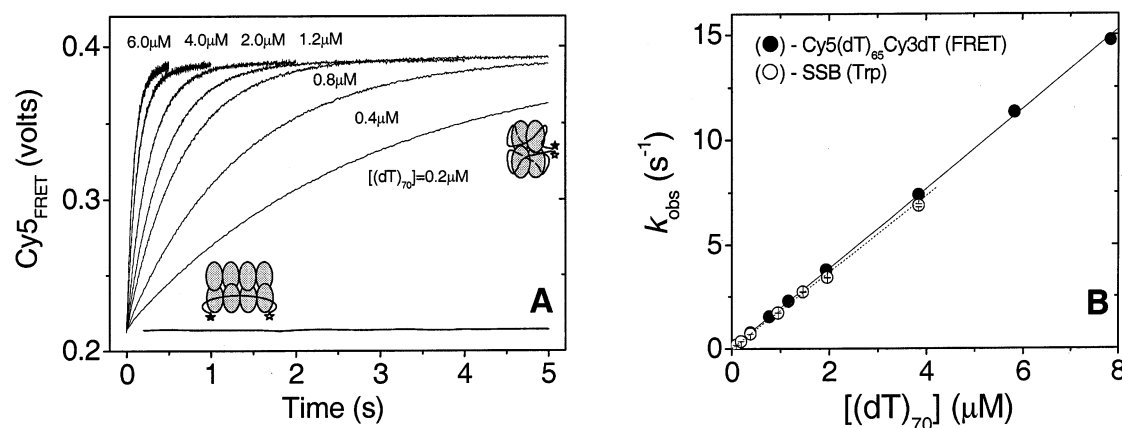
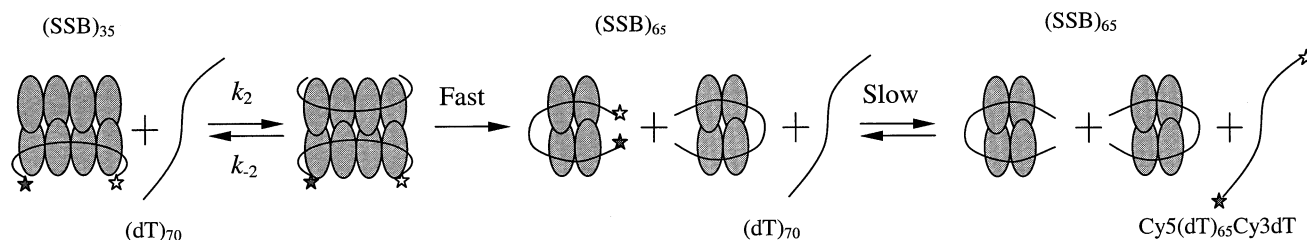


FIGURE 9: Kinetics of the transition from an $(SSB)_{35}$ complex [2:1 $SSB-Cy5(dT)_{65}Cy3dT$ complex] to a 1:1 $(SSB)_{65}$ complex upon addition of excess $(dT)_{70}$ by monitoring Cy5 FRET. (A) Cy5 FRET fluorescence time courses obtained upon mixing the $SSB-Cy5(dT)_{65}Cy3dT$ complex (40 and 10 nM, respectively) with increasing concentrations of $(dT)_{70}$ (0.02 M NaCl, buffer T, pH 8.1, 25 °C). The concentration of $(dT)_{70}$ was varied from 0.2 to 8 μM (final concentrations). Each time course was fit to a single-exponential decay using eq 1 (with $n = 1$) to obtain k_{obs} . The fits are indistinguishable from the traces shown, but are not shown in the figure. The increase in the magnitude of the Cy5 FRET signal corresponds to the transition from a 2:1 $(SSB)_{35}$ complex in which two SSB tetramers are bound to $Cy5(dT)_{65}Cy3dT$ to the $(SSB)_{65}$ complex in which one $Cy5(dT)_{65}Cy3dT$ molecule is bound to one SSB tetramer. (B) Dependence on $[(dT)_{70}]$ of k_{obs} obtained from the single-exponential fits of the Cy5 FRET time courses shown in panel A (●) and dependence on $[(dT)_{70}]$ of k_{obs} obtained from similar experiments as in panel A, but by monitoring the changes in SSB Trp fluorescence quenching (○).

Scheme 5



between the ends of the highly flexible ssDNA decreases with increasing salt concentration, due to an electrostatic screening of the phosphate charges in the DNA.

To examine the kinetics of SSB transfer from cooperatively bound $(SSB)_{35}$ complexes, we premixed 10 nM $Cy5(dT)_{65}Cy3dT$ with 40 nM SSB tetramer in 20 mM NaCl (buffer T, pH 8.1, 25 °C) so that the initial complex consists of two tetramers bound to the ssDNA in the $(SSB)_{35}$ binding mode. The resulting changes in the Cy5 FRET signal were then monitored in a stopped-flow experiment upon addition of an excess of unlabeled $(dT)_{70}$. Figure 9A shows stopped-flow traces obtained after mixing the $SSB-ssDNA$ complex with varying concentrations of $(dT)_{70}$ (from 0.2 to 6 μM). Each time course shows a single exponential increase (~ 2 -fold) in the magnitude of the Cy5 FRET signal. The observed rates (k_{obs}) increase linearly with increasing $(dT)_{70}$ concentrations as shown in Figure 9B, indicating that dissociation of SSB from the 2:1 $(SSB)_{35}$ complex occurs via the transient formation of an intermediate in which two ssDNA molecules are bound to at least one SSB tetramer (possibly both). The slope of the line in Figure 9B [$(1.90 \pm 0.02) \times 10^6 M^{-1} s^{-1}$] is the apparent bimolecular rate constant for the binding of unlabeled $(dT)_{70}$ to the $(SSB)_{35}$ complex. Similar experiments monitoring the additional SSB Trp fluorescence (~ 35 –40%) quenching that accompanies the transition from the $(SSB)_{35}$ to the $(SSB)_{65}$ complex (7) show the same dependence of k_{obs} on $[(dT)_{70}]$ with a nearly identical slope of $(1.78 \pm 0.02) \times 10^6 M^{-1} s^{-1}$ (see Figure 9B).

The final plateau value in the time courses shown in Figure 9A corresponds to the expected FRET signal when

$Cy5(dT)_{65}Cy3dT$ is fully wrapped around a single SSB tetramer in the $(SSB)_{65}$ binding mode. Therefore, it appears that after the unlabeled $(dT)_{70}$ binds to the SSB tetramers in complex with the $Cy5(dT)_{65}Cy3dT$ DNA, further fast reorganization of the complexes occurs, resulting in the formation of 1:1 fully wrapped complexes at equilibrium. This is indicated in the kinetic pathway shown in Scheme 5, where the binding of the second ssDNA molecule induces a very fast (probably irreversible) disproportionation reaction to form two $(SSB)_{65}$ complexes. The rate of dissociation of $(dT)_{70}$ from these $(SSB)_{65}$ complexes is very slow ($\sim 5 \times 10^{-4} s^{-1}$) under these low-salt conditions (20 mM NaCl), based on the data obtained with $F(dT)_{70}$ (see the inset of Figure 4A). This would explain why we do not see any appreciable dissociation of $Cy5(dT)_{65}Cy3dT$ from the 1:1 $(SSB)_{65}$ complexes at longer times even upon introducing a very large excess of competitor $(dT)_{70}$ (i.e., there is no slow decrease in the magnitude of the Cy5 FRET signal after the plateau value is reached in the time courses in Figure 9A). However, the rate of dissociation of $Cy5(dT)_{65}Cy3dT$ from a 1:1 $(SSB)_{65}$ complex is expected to increase with increasing salt concentrations. Therefore, if upon addition of the excess unlabeled $(dT)_{70}$ to the $(SSB)_{35}$ complex in 20 mM NaCl we also increase [NaCl], then we might observe dissociation of $Cy5(dT)_{65}Cy3dT$ following the rapid formation of the $(SSB)_{65}$ complexes. Curve 5 in Figure 8 shows the time course from such a stopped-flow experiment in which a preformed $(SSB)_{35}$ complex (10 nM $Cy5(dT)_{65}Cy3dT$ and 40 nM SSB final concentrations) in 20 mM NaCl was mixed with a large excess of $(dT)_{70}$ (10 μM) in 1.0 M NaCl, yielding

final concentrations of 5 μM (dT)₇₀ and 0.5 M NaCl. Within 100 ms, the magnitude of the Cy5 FRET signal increases, indicating formation of a 1:1 (SSB)₆₅ complex with the Cy5(dT)₆₅Cy3dT DNA, but this is followed by a much slower decrease in the magnitude of the Cy5 FRET signal, reflecting dissociation of Cy5(dT)₆₅Cy3dT from the complex with an observed dissociation rate of 0.023 s⁻¹. As expected, this rate falls between the values of 0.051 and 0.007 s⁻¹ measured in 0.8 and 0.2 M NaCl, respectively, for the dissociation of F(dT)₇₀ from a 1:1 fully wrapped SSB complex induced by the addition of an excess of 5 μM (dT)₇₀ (see Figure 4A).

DISCUSSION

Direct transfer of proteins between DNA sites, or inter-segment transfer, has been reported for a number of proteins, including *E. coli lac* repressor (32), *E. coli* SSB (20), *E. coli recA* protein (33), and histones (34), as well as the DNA intercalating dye ethidium (35). Direct transfer of the homotetrameric *lac* repressor, along with one-dimensional sliding of the protein, has been postulated to play a role in the mechanisms by which this gene regulatory protein can locate its specific DNA binding site, the *lac* operator, when it is embedded within a large region of otherwise nonspecific DNA (36, 37).

On the basis of nitrocellulose filter binding studies of the kinetics of dissociation of *E. coli* SSB from natural ssDNA, Schneider and Wetmur (20) concluded that clusters of SSB could be transferred from one ssDNA molecule to another without proceeding through a free SSB intermediate. These conclusions were based on analyses of the magnitude of the dissociation rate constant and its dependence on solution viscosity, temperature, and the length of the acceptor ssDNA molecules. Although the evidence for such a direct transfer reaction is good, one major test of such a mechanism not performed by Schneider and Wetmur (20) is that the rate of ssDNA dissociation should increase with acceptor DNA concentration. Furthermore, since the ability of the *E. coli* SSB tetramer to form different binding modes on long ssDNA had not been recognized at the time of these first experiments, the influence that the different SSB binding modes might have on such transfer reactions had not been assessed. For these reasons as well as to obtain detailed kinetic information about the rates, intermediates, and rate-limiting steps involved in such a direct transfer reaction, we have performed detailed stopped-flow studies of the kinetics of transfer of SSB between two DNA molecules. These studies were designed to examine the kinetic mechanism of transfer of individual SSB tetramers from well-defined complexes of SSB formed in its different binding modes using ss oligodeoxythymidylates while monitoring intrinsic fluorescent signals from the SSB (Trp residues) as well as extrinsic fluorescence probes attached to the ssDNA.


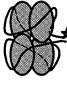

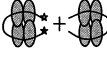
The kinetic competition experiments reported here provide clear evidence that the *E. coli* SSB tetramer can be transferred directly from one ssDNA molecule to another without proceeding through a free protein intermediate. This direct transfer reaction proceeds through a doubly ligated SSB intermediate (DPD* in Schemes 1, 3, and 4) in which the SSB tetramer is transiently bound to the two ssDNA molecules simultaneously. We have shown previously that the

binding of the first ssDNA molecule to an SSB tetramer occurs with a very rapid, nearly diffusion controlled rate (24). Since each SSB tetramer has four potential binding sites for ssDNA, binding of a second ssDNA molecule is possible (although with a lower rate) if some of the SSB subunits are not involved in direct binding interactions with the first ssDNA molecule. Once the doubly ligated (DPD*) complex is formed, both ssDNA molecules have the potential to dissociate from the complex with equal probability if the DNA molecules are identical. If dissociation of the first ssDNA molecule occurs, then the SSB remains bound to the second DNA molecule and the direct transfer reaction is completed. In general, the ssDNA that is present in larger excess will determine the net direction of the process. In our case, the reaction is set up to proceed in the direction of net formation of the complex with unlabeled ssDNA which will be accompanied by the release of labeled ssDNA* into solution.

The major evidence for this type of direct transfer process is that the observed rate of dissociation, k_{obs} , of a fluorescently labeled donor ssDNA (D*) from the SSB tetramer increases with increasing concentrations of an unlabeled acceptor ssDNA. This increase in k_{obs} is linearly dependent on [D] when [D] \gg [D*]. This type of reaction pathway requires a DNA binding protein to possess multiple (at least two) DNA binding sites. In fact, early studies by Schneider and Wetmur (20) with *E. coli* SSB bound to ssDNA (375 nucleotides) much longer than those used in our experiments indicated that SSB could undergo such a direct transfer reaction. In the experiments reported here, we have studied the direct transfer of individual SSB tetramers starting with well-defined SSB complexes formed with much shorter oligodeoxythymidylates [(dT)₃₅ and (dT)₇₀]. In this way, we could examine the effect on the rate of the transfer reaction of the availability of free SSB subunits in the preformed SSB–ssDNA complex. The use of these well-defined complexes enabled us to obtain quantitative information about the rate constants for many of the steps along the reaction pathway, to determine the rate-limiting steps, and to understand how these rates are influenced by the type of complex formed and the solution conditions under which the reaction occurs.

Direct Transfer Requires the Availability of Free ssDNA Binding Sites on the SSB Tetramer. Our results clearly indicate that a direct transfer reaction requires that the SSB–D* complex have unoccupied DNA binding sites available for the binding of the acceptor ssDNA. This conclusion is evident by the large differences in the rates of SSB transfer when the SSB complex was initially formed with donor strands of (dT)₃₅ versus (dT)₇₀. Table 5 compares the rate constants for the direct transfer reaction for these SSB–donor DNA complexes. Under all salt conditions in which a 1:1 SSB–donor DNA complex is preformed, the observed rate of binding the acceptor DNA is much slower when the donor strand is (dT)₇₀. At 200 mM NaCl and 0.4 M NaBr, the rates are $>5 \times 10^4$ - and $\sim 5 \times 10^3$ -fold slower, respectively (compare columns 2 and 5 of Table 5). At 20 mM NaCl, direct transfer is so slow from a 1:1 SSB–(dT)₇₀ complex that it is undetectable, whereas the apparent rate constant for binding an acceptor ssDNA to a 1:1 SSB–(dT)₃₅ complex is $3.3 \times 10^6 \text{ M}^{-1} \text{ s}^{-1}$ under the same conditions. These large differences appear to reflect the fact that the rate of binding

Table 5: Binding and Dissociation Rates for Direct Transfer of SSB from Preformed (SSB)₃₅ and (SSB)₆₅ Complexes^a

Preformed complexes	 (SSB) ₃₅ SSB-F(dT) ₃₅			 (SSB) ₆₅ SSB-F(dT) ₇₀			 (SSB) ₃₅ SSB-Cy5(dT) ₆₅ Cy3dT	
	(dT) ₃₅ Binding		Dissociation	(dT) ₇₀ Binding		Dissociation	(dT) ₇₀ Binding	SSB Dissociation
	k_2 (M ⁻¹ s ⁻¹)	$k_2[D]_{\max}$ (s ⁻¹)	k_{-2} RATE LIMITING (s ⁻¹)	$k_{2,app}$ (M ⁻¹ s ⁻¹)	$k_{2,app}[D]_{\max}$ RATE LIMITING (s ⁻¹)	k_{-2} (s ⁻¹)	k_2 (M ⁻¹ s ⁻¹)	
0.02 M NaCl	(3.3±0.9)×10 ⁶	~23	~0.3	-	-	- ($k_{-1} \approx 5 \times 10^{-4}$)	(1.8-1.9)×10 ⁶	Very fast
0.2 M NaCl	>6.3×10 ⁷	>250	~0.1	(1.2±0.1)×10 ³	~0.012	>>0.012	-	-
0.4 M NaBr	(2.6±0.1)×10 ⁷	~100	~1.6	(5.1±0.3)×10 ³	~0.10	>>0.10	-	-

^a Conditions: buffer T, pH 8.1, 25 °C. Rate constants are defined as in Schemes 1 and 2.

ssDNA to a preformed 1:1 SSB-(dT)₇₀ complex is limited by access of the acceptor strand to unoccupied SSB subunits. The much slower rates of binding reflect the fact that only ~0.02% (at 0.4 M NaBr) and ~0.002% (at 0.2 M NaCl) of the population of the SSB-(dT)₇₀ complexes have unligated subunits available for binding of a second ssDNA molecule.

In Table 5, we also compare the observed second-order rate constant for an acceptor ssDNA binding to a complex of two SSB tetramers bound cooperatively to a (dT)₇₀ molecule in the (SSB)₃₅ binding mode. The observed second-order rate constant is $\sim 2 \times 10^6 \text{ M}^{-1} \text{ s}^{-1}$, which is very close to the observed second-order rate constant for ssDNA binding to a single tetramer in the (SSB)₃₅ mode [i.e., a 1:1 SSB-(dT)₃₅ complex]. These two rate constants are presumably comparable since both SSB-donor DNA complexes have half of their SSB subunits free and thus available for acceptor ssDNA binding.

It is also of interest to compare the apparent bimolecular rate constants for binding of a second molecule of DNA to an SSB tetramer with that for binding of the first molecule of DNA. We have previously measured the apparent bimolecular rate constant, $k_{1,app}$, for binding (dT)₇₀ and (dT)₃₅ to a free SSB tetramer over a range of salt concentrations (24). In 0.2 M NaCl (buffer T, pH 8.1, 25 °C) we find $k_{1,app} = (9.5 \pm 0.30) \times 10^8$ and $(9.2 \pm 0.3) \times 10^8 \text{ M}^{-1} \text{ s}^{-1}$ for (dT)₇₀ and (dT)₃₅, respectively. Under the same conditions, the apparent bimolecular rate constant for binding a second molecule of (dT)₃₅ to a 1:1 SSB-(dT)₃₅ complex is slightly lower, with a $k_{2,app}$ of $(1.03 \pm 0.04) \times 10^8 \text{ M}^{-1} \text{ s}^{-1}$. The latter rate constant is consistent with those estimated for (dT)₃₅ binding to the open site on a 1:1 SSB-(dT)₃₅ complex from the direct transfer experiments reported here (see column 2 of Table 5). It is also notable that the bimolecular rate constant for formation of a singly ligated SSB-(dT)₇₀ complex decreases with increasing monovalent salt concentrations (24). In contrast, increasing monovalent salt concentrations facilitate the rate of formation of a doubly ligated intermediate. For the SSB-F(dT)₃₅ complex, this rate (k_2) increases more than 20-fold when [NaCl] increases from 20

to 200 mM (see Table 5), and for the SSB-F(dT)₇₀ complex, the apparent rate constant ($k_{2,app}$) increases 10-fold when [NaCl] increases from 0.2 to 1 M or [NaBr] from 0.4 to 2.0 M (see Table 1). The molecular basis for these qualitatively different effects of salt concentration on $k_{1,app}$ and $k_{2,app}$ is likely the same as the basis for the strong negative cooperativity that is observed for the equilibrium binding of a second ssDNA to an SSB tetramer. It has been shown that the equilibrium binding of two molecules of (dT)₃₅ to the SSB tetramer occurs with negative cooperativity and that this negative cooperativity decreases with increasing salt concentrations (16, 17, 30, 31).

Rate-Limiting Steps in the Direct Transfer Reaction. The transfer of SSB from one DNA molecule to another always occurs through a doubly ligated SSB intermediate (see Schemes 1, 3, and 4). However, the rate-limiting step governing the overall transfer process differs depending on whether the starting SSB complex has any unoccupied DNA binding sites. For example, when the starting complex is a 1:1 SSB-(dT)₇₀ fully wrapped complex [(SSB)₆₅ mode], then the rate of transfer is limited by the rate of binding of the second DNA molecule, which is in turn limited by the access to an unoccupied DNA binding site on the SSB tetramer. This is illustrated in Table 5, where we see that the maximum observed rate of formation of a doubly ligated SSB complex for (dT)₇₀ binding to the SSB-F(dT)₇₀ complex ($k_2[D]_{\max}$) does not exceed 0.1 s⁻¹ (see column 6 of Table 5) even at the maximum concentration of (dT)₇₀ used in these experiments ($\approx 20 \mu\text{M}$), which indicates that dissociation of F(dT)₇₀ from the doubly ligated complex occurs with a rate of $\gg 0.1 \text{ s}^{-1}$. On the other hand, when the starting complex is a 1:1 SSB-(dT)₃₅ complex or a 2:1 SSB-(dT)₇₀ complex, both of which have half of the subunits on the SSB tetramer unoccupied, then the acceptor ssDNA can bind rapidly to form the doubly ligated (DPD*) intermediate; however, the rate of transfer is now limited by the rate of dissociation of the donor ssDNA molecule (see Table 5). For example, when one starts with SSB-F(dT)₃₅ complexes formed in NaCl, the formation of a doubly ligated intermediate occurs with

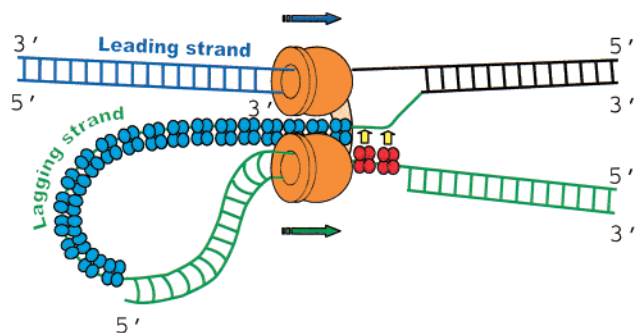


FIGURE 10: Possible use of a direct transfer mechanism to recycle SSB tetramers from old to new lagging strand ssDNA during DNA replication. Two pol III holoenzymes (orange) are depicted in the process of replicating the leading (blue) and lagging (green) strands of DNA. SSB tetramers bound in the (SSB)₃₅ binding mode (via two subunits) to the newly formed lagging strand ssDNA are shown in cyan, whereas the SSB bound to the old lagging strand ssDNA upon which replication has almost been completed is shown in red. The SSB tetramers in red will be transferred to the new lagging strand ssDNA by a direct transfer mechanism (shown by yellow arrows).

observed rates of ~ 23 and >250 s⁻¹ at the highest competitor concentrations used in our experiments [≈ 7 μ M (dT)₃₅ in 20 mM NaCl and 4 μ M (dT)₃₅ in 0.2 M NaCl, respectively] (see column 3 of Table 5). However, the rate constants for dissociation of F(dT)₃₅ from these complexes do not exceed 0.3 and 0.1 s⁻¹, respectively (see column 4 of Table 5).

Implications of a Direct Transfer Mechanism for Recycling of *E. coli* SSB during Lagging Strand DNA Replication. What might be the potential utility of a direct transfer mechanism for SSB function? The majority of the SSB that functions during DNA replication is thought to bind to the ssDNA that is transiently formed on the lagging strand. The SSB is believed to coat the template ssDNA ahead of the lagging strand DNA polymerase III holoenzyme that must continuously reinitiate DNA synthesis at the sites of the RNA primers on the lagging strand (38). Of course, all of this SSB must eventually be displaced for the DNA polymerase to carry out DNA synthesis. Furthermore, this displaced SSB must be recycled and thus rebind the lagging strand ssDNA segment that is being newly formed behind the lagging strand DNA polymerase. If, to be recycled, the SSB is required to dissociate from the old lagging strand and rebind to the new lagging strand via a free protein intermediate, then this recycling could be quite slow if the free SSB concentration is low. It is difficult to establish the concentration of free SSB during DNA replication. Estimates of the total amount of SSB in *E. coli* have ranged from ~ 300 to 2×10^3 tetramers per cell (2), corresponding to concentrations of ~ 0.05 – 0.3 μ M. The lower end of this estimate would be enough SSB to coat the ssDNA that is transiently formed during replication, but there would be little excess free protein. Hence, recycling via a free protein intermediate might be quite slow. One way to avoid such a slow step would be to use a direct transfer mechanism to move SSB tetramers from the old ssDNA to the newly formed ssDNA on the lagging strand as depicted schematically in Figure 10. In fact, since it is proposed that the lagging strand is looped as depicted in Figure 10, then the SSB on the old ssDNA could be positioned adjacent to the newly formed ssDNA, and thus, the new ssDNA could transiently bind the unoccupied subunits of the SSB tetramers on the old ssDNA.

Of course, this would require that the SSB tetramer be bound on the ssDNA in its cooperative (SSB)₃₅ binding mode with two of its subunits unoccupied. If the SSB tetramer were bound in the fully wrapped (SSB)₆₅ mode, then as we have shown here, the rate of direct transfer would be limited by the need to partially dissociate ssDNA from the SSB tetramer to expose a ssDNA binding site. In fact, this scenario suggests that direct transfer would be most likely if the mode of SSB binding on the lagging strand were the cooperative (SSB)₃₅ binding mode.

ACKNOWLEDGMENT

We thank Dr. Peter Burgers and Dr. Michael O'Donnell for discussions about the potential roles of SSB direct transfer during DNA replication, Dr. Chris Fischer and Aaron Lucius for comments on the manuscript, and T. Ho for synthesis and purification of the oligodeoxynucleotides used in this study.

REFERENCES

- Chase, J. W., and Williams, K. R. (1986) *Annu. Rev. Biochem.* 55, 103–136.
- Meyer, R. R., and Laine, P. S. (1990) *Microbiol. Rev.* 54, 342–380.
- Lohman, T. M., Bujalowski, W., and Overman, L. B. (1988) *Trends Biochem. Sci.* 13, 250–255.
- Lohman, T. M., and Bujalowski, W. (1990) in *The Biology of Nonspecific DNA-Protein Interactions* (Revzin, A., Ed.) pp 131–170, CRC Press, Boca Raton, FL.
- Greipel, J., Urbanke, C., and Maass, G. (1989) in *Protein-Nucleic Acid Interaction* (Saenger, W., and Heinemann, U., Eds.) pp 61–86, CRC Press, Boca Raton, FL.
- Lohman, T. M., and Ferrari, M. E. (1994) *Annu. Rev. Biochem.* 63, 527–570.
- Lohman, T. M., and Overman, L. B. (1985) *J. Biol. Chem.* 260, 3594–3603.
- Bujalowski, W., and Lohman, T. M. (1986) *Biochemistry* 25, 7799–7802.
- Bujalowski, W., Overman, L. B., and Lohman, T. M. (1988) *J. Biol. Chem.* 263, 4629–4640.
- Griffith, J. D., Harris, L. D., and Register, J., III (1984) *Cold Spring Harbor Symp. Quant. Biol.* 49, 553–559.
- Lohman, T. M., Overman, L. B., and Datta, S. (1986) *J. Mol. Biol.* 187, 603–615.
- Ferrari, M. E., Bujalowski, W., and Lohman, T. M. (1994) *J. Mol. Biol.* 236, 106–123.
- Wei, T.-F., Bujalowski, W., and Lohman, T. M. (1992) *Biochemistry* 31, 6166–6174.
- Bujalowski, W., and Lohman, T. M. (1987) *J. Mol. Biol.* 195, 897–907.
- Overman, L. B., Bujalowski, W., and Lohman, T. M. (1988) *Biochemistry* 27, 456–471.
- Bujalowski, W., and Lohman, T. M. (1989) *J. Mol. Biol.* 207, 249–268.
- Bujalowski, W., and Lohman, T. M. (1989) *J. Mol. Biol.* 207, 269–288.
- Raghunathan, S., Kozlov, A. G., Lohman, T. M., and Waksman, G. (2000) *Nat. Struct. Biol.* 7, 648–652.
- Romer, R., Schomburg, U., Krauss, G., and Maass, G. (1984) *Biochemistry* 23, 6132–6137.
- Schneider, R. J., and Wetmur, J. G. (1982) *Biochemistry* 21, 608–615.
- Urbanke, C., and Schaper, A. (1990) *Biochemistry* 29, 1744–1749.
- Lohman, T. M. (1986) in *Kinetics of protein-nucleic acid interactions: Use of salt effects to probe mechanisms of interaction*, pp 191–245, CRC Press, Boca Raton, FL.
- Krauss, G., Sindermann, H., Schomburg, U., and Maass, G. (1981) *Biochemistry* 20, 5346–5352.
- Kozlov, A. G., and Lohman, T. M. (2002) *Biochemistry* 41, 6032–6044.
- Lohman, T. M., Green, J. M., and Beyer, S. (1986) *Biochemistry* 25, 21–25.

26. Bujalowski, W., and Lohman, T. M. (1991) *J. Biol. Chem.* 266, 1616–1626.
27. Kowalczykowski, S. C., Lonberg, N., Newport, J. W., and von Hippel, P. H. (1981) *J. Mol. Biol.* 145, 75–104.
28. Ferrari, M. E., and Lohman, T. M. (1994) *Biochemistry* 33, 12896–12910.
29. Johnson, K. A. (1986) *Methods Enzymol.* 134, 677–702.
30. Kozlov, A. G., and Lohman, T. M. (1998) *J. Mol. Biol.* 278, 997–1012.
31. Lohman, T. M., and Bujalowski, W. (1988) *Biochemistry* 27, 2260–2265.
32. Ruusala, T., and Crothers, D. M. (1992) *Proc. Natl. Acad. Sci. U.S.A.* 89, 4903–4907.
33. Menetski, J. P., and Kowalczykowski, S. C. (1987) *J. Biol. Chem.* 262, 2085–2092.
34. Aragay, A. M., Dias, P., and Daban, J.-R. (1988) *J. Mol. Biol.* 204, 141–154.
35. Bresloff, J. L., and Crothers, D. M. (1975) *J. Mol. Biol.* 95, 103.
36. von Hippel, P. H., and Berg, O. G. (1989) *J. Biol. Chem.* 264, 675–678.
37. Berg, O. G., and von Hippel, P. H. (1985) *Annu. Rev. Biophys. Chem.* 14, 131–160.
38. Kelman, Z., and O'Donnell, M. (1995) *Annu. Rev. Biochem.* 64, 171–200.

BI020361M